Research Square

Preprints are preliminary reports that have not undergone peer review.
They should not be considered conclusive, used to inform clinical practice,
or referenced by the media as validated information.

NuMA1 controls myonuclear motility in striated skeletal muscle through AMPK activity and is impaired in Duchenne Muscular Dystrophy

Vincent Gache

vincent.gache@inserm.fr

Institut NeuroMyoGène, Physiopathologie et Génétique du Neurone et du Muscle, UMR CNRS 5261 – INSERM U1315, Université Claude Bernard Lyon 1 https://orcid.org/0000-0002-2928-791X

Nathalie Couturier

Institut NeuroMyoGène, Physiopathologie et Génétique du Neurone et du Muscle, UMR CNRS 5261 – INSERM U1315, Université Claude Bernard Lyon 1

Léa Castellano

Institut NeuroMyoGène, Physiopathologie et Génétique du Neurone et du Muscle, UMR CNRS 5261 – INSERM U1315, Université Claude Bernard Lyon 1

Alireza Ghasemizadeh

Institut NeuroMyoGène, Physiopathologie et Génétique du Neurone et du Muscle, UMR CNRS 5261 – INSERM U1315, Université Claude Bernard Lyon 1

Emilie Christin

INSERM/INMG

Céline Malleval

Institut NeuroMyoGène, Physiopathologie et Génétique du Neurone et du Muscle, UMR CNRS 5261 – INSERM U1315, Université Claude Bernard Lyon 1

Alexandre Janin

INSERM/INMG https://orcid.org/0000-0003-3571-003X

Gaëtan Juban

Institut NeuroMyoGène - Physiopathologie et Génétique du Neurone et du Muscle / Université Claude Bernard Lyon 1 / Inserm U1315 / CNRS UMR 5261

Alexis Osseni Osseni

INMG-PGNM https://orcid.org/0000-0003-3435-5785

Jean-Luc Thomas

INSERM/INMG

Konig Stephane

Faculty of Medicine, University of Geneva https://orcid.org/0000-0002-0801-279X

Jessica Brunetti

Université de genève/Facultyof medicine

Alexandra Kraut

Exploring the Dynamics of Proteomes (EDyP) Laboratoire Biologie à Grande Echelle (BGE)

Yohann Couté

Grenoble Alpes University, CEA, INSERM, UA13 BGE, CNRS, CEA, UAR2048

Nathalie Streichenberger

Department of Neuropathology, Groupe Hospitalier Est, Hospices Civils de Lyon

Rémi Mounier

CNRS https://orcid.org/0000-0003-3464-3322

Article

Keywords:

Posted Date: September 29th, 2025

DOI: https://doi.org/10.21203/rs.3.rs-7713210/v1

License: This work is licensed under a Creative Commons Attribution 4.0 International License.
Read Full License

Additional Declarations: There is **NO** Competing Interest.

Version of Record: A version of this preprint was published at Cell Death & Disease on June 17th, 2026.
See the published version at https://doi.org/10.1038/s41419-026-08987-5.

NuMA1 controls myonuclear motility in striated skeletal muscle through AMPK activity and is impaired in Duchenne Muscular Dystrophy.

Nathalie Couturier[1*], Léa Castellano[1*], Alireza Ghasemizadeh[1], Emilie Christin[1], Céline Malleval[1], Alexandre Janin[1], Gaëtan Juban[1], Alexis Osseni[1], Jean-Luc Thomas[1], Stéphane Koenig[2], Jessica Brunetti[2], Alexandra Kraut[3], Yohann Couté[3], Nathalie Streichenberger[1,4], Rémi Mounier[1] and Vincent Gache[1].

* Contributed equally

1- Institut NeuroMyoGène, Physiopathologie et Génétique du Neurone et du Muscle, UMR CNRS 5261 – INSERM U1315, Université Claude Bernard Lyon 1, Lyon, France, 8 Avenue Rockefeller, 69373, Lyon Cedex 08, France.

2- Department of Cell Physiology and Metabolism. Geneva Medical Center, 1, Rue Michel Servet, 1211 Geneva 4, Switzerland.

3- Grenoble Alpes University, CEA, INSERM, UA13 BGE, CNRS, CEA, UAR2048, F-38000 Grenoble, France.

4- Department of Neuropathology, Groupe Hospitalier Est, Hospices Civils de Lyon, Bron, France

Corresponding author: vincent.gache@inserm.fr

Abstract

Skeletal muscle consists in a bundle of thousands post-mitotic multinucleated cells, called myofibers, in which myonuclei are evenly spaced and positioned at the periphery. This myonuclear positioning i) shapes myonuclear domain (MND) in myofibers, essential for the transcriptional integrity of myofibers, ii) is driven by cytoskeleton and associated proteins and iii) is required for proper myofiber functions. In numerous of muscle diseases (*i.e.* myopathies), alteration of myonuclei localization (internalized and/or mispositioned) contributes to myofiber misfunctioning, supporting the need to better understand the fundamental mechanisms that regulates myonuclei dynamics and to restore the establishment of myonuclear domains in these

diseases. In this study, we show that in Duchenne muscular dystrophy (DMD) myofibers, myonuclei are more dynamic and contribute to the failure in MNDs settings, suggesting that in pathological conditions enhanced myonuclear motility impact myonuclear distribution. To identify new actors regulating this MND settings, we performed a mass spectrometry (MS)-based proteomic analysis to identify microtubule associated proteins (MAPs) in myotubes/myofibers and performed a siRNA screening on selected candidates. This approach allowed to highlight NuMA1 as a new factor controlling myoblast fusion and myonuclear positioning through the control of nuclear-microtubule-organizing-center (n-MTOC) integrity and microtubule network orientation. Strikingly, while NuMA1 is restrained to myonuclei in mononucleated myoblasts, it progressively accumulates in the cytoplasm during muscle cell differentiation, preferentially with microtubule (MT) nucleation spots at the vicinity of the nuclear membrane. We identified that AMP Kinase activity has an essential role in NuMA1 nuclear accumulation through the specific phosphorylation on serine-1853 and the ability of myonuclei to accumulate NuMA1 is correlated to their motility in myofibers. Finally, we show that nuclear NuMA1 content is increased in DMD patients and *mdx* mouse model, contributing to more dynamic myonuclei that can manipulated pharmacologically through the control of AMPK activity. Altogether, our data identify a novel mechanism by which nuclear sequestration of a MAP allows to couple nuclear positioning and motion to MT organization.

Introduction

The positioning of nuclei in large post-mitotic syncytium, such as in skeletal muscle cells, is a challenging process as these cells contained thousands of nuclei in which positioning controls muscle cells functionality[1,2]. Nuclear positioning is an active process, controlling cells fate determination and involving mechanical interplays between nuclear envelope proteins and cytoskeleton networks[3]. Microtubule (MT) network appears as a key player in the regulation of nuclear positioning settings in the majority of cells[4].

Most differentiated cells, including muscle cells, epithelial cells and neurons, set up “non-centrosomal” MTOC (ncMTOC) allowing the nucleation/assembly of MTs at a certain distance from the nucleus, leading to alternative patterns, orientation/polarization of the MT network[5–7]. The expression of various MT-interacting proteins along skeletal muscle cells differentiation carries out myonuclei positioning through the control/maintenance of newly formed MT network architecture[8]. Previously, a limited number of MAPs and molecular motors has been

identified controlling myonuclei motion and thus myonuclei spreading in developing muscle cells[1,9–12].

We showed that in mature myofibers, enhanced myonuclei velocity is correlates with a delay in the formation/maturation of organelles such as the sarcoplasmic reticulum and can ultimately lead to internalized myonuclei within myofibers, associated with transcriptional activity misregulation[13,14]. In addition, myonuclei displacement into mature myofibers can reveal local ongoing processes such as muscle cell reparation[15]. However, it is still puzzling how myonuclei remain anchored in specific localizations along mature mammalian skeletal muscle fibers and what are the functional consequences of positioning/shape alterations. In pathological conditions such as in Duchenne Muscular Dystrophy (DMD), it is common to find merging/aggregated myonuclei with various shapes and orientations along mature myofiber[16–18]. Interestingly, myonuclei velocity or time-in-motion in developing myofibers fluctuates depending on the developmental phase, the presence of myofibrils and are far from being homogenous between myonuclei in the same myotubes/myofibers and so far, no specific marker has been identified that reveal myonuclei motility[1,9,13,19]. Here, we confirm the correlation between alteration of myonuclei velocity and muscle pathological conditions (DMD) and provide a new mechanism for the regulation of nuclear movement inside myofibers and the identification of marker reflecting myonuclei motility.

Results

Myonuclear velocity/displacement is enhanced in Duchenne Muscular Dystrophy myofibers

DMD is caused by mutations in the *DMD* gene, encoding the dystrophin protein, previously identified as a MAP[20]. Indeed, in *mdx* mice, a well-established model of human DMD, MT network organization in skeletal muscle cells is dramatically altered[21]. To investigate the relationship between nuclear positioning and MT network impairment, we isolated *Tibialis Anterior* muscle fibers from 2 months-old WT and *mdx* mice (Fig.1a-d). We first confirmed MT network disorganization in *mdx* muscle fibers (Fig.1b) and found that the distance between myonuclei in *mdx* muscle fibers was decreased by more than 20%, reflecting a reduction in MND size (Fig.1c). Interestingly, myonuclei circularity is increased by more than 15% in *mdx* muscle fibers compared with the WT condition, indicating altered global mechanical tension applied on each myonucleus, which consequently appeared rounder (Fig.1b, d).

To determine whether myonuclei shape alterations reflect a failure in myonuclear velocity that impairs MND settings[13], we isolated primary myoblasts from WT and *mdx* mice pups (age P4-6) and transfected the cells with a TagRFP-lamin-chromobody® plasmid to visualize myonuclei shape and displacement. Myoblasts were further induced to fuse to form myotubes, which were maturated into myofibers using a Matrigel® sandwich culture[22] (Fig.1e). We next performed time-lapse confocal microscopy (Fig.1f) and tracked myonuclei in these *in vitro* myofibers (Fig.1g-j). First, quantification of myonuclear circularity revealed that deformation of myonuclei is an early event, with a nearly 10% increase in myonuclei circularity in *mdx* myofibers compared to controls (Fig.1g). Myonuclear displacement analysis showed that, in control condition, myonuclei alternate between phases of movement and pauses. Myonuclear motion occurred at a median speed of 0,21 ± 0,01 µm/min, with pauses lasting approximately 5 hours per day, resulting in a median daily displacement of around 150 µm (Fig.1h-i, supplementary Fig.1a-b). In *mdx* myofibers, pause duration was decreased by more than half (supplementary Fig.1b), while median speed increased to 0,43 ± 0,01 µm/min, yielding an average daily displacement of up to 500 µm (Fig.1h-i, supplementary Fig.1a-b). Interestingly, this enhancement of myonuclei velocity correlated with a failure to correctly align myonuclei, which appeared aggregated in more than half of myofibers (Fig.1j). Altogether, our data suggest that rounder myonuclei reflect more displacement of myonuclei in mature myofibers and confirm that the increased myonuclear velocity observed in *mdx* myofibers leads to alterations in MND organization in myofibers.

NuMA1 is required for myonuclear positioning during myofiber formation

Myonuclei displacement in myofibers has primarily been linked to interactors of the MT network[1,9,13,15,23]. To identify new factors that interact early with, and regulate, MT network architecture while contributing to the MND organization during myofiber formation, we purified MAPs from either 3-days primary myotubes or 10-days primary myofibers. MT-interacting proteins were identified using MS-based proteomics, enabling classification according to their enrichment in immature (myotubes) or mature (myofibers) stages (Supplementary Fig.1c-e, Table1). Among the 2037 proteins identified, we selected 66 candidates and tested their involvement in myonuclear spreading using pools of 3 specific siRNAs (Table2). Approximately half of the candidates, when silenced, caused defective myonuclear alignment during the early steps of myotube formation (Supplementary Fig.1e). Notably, this targeted siRNA screen revealed a critical role for *Numa1*, whose down-regulation

produced a more severe defect than the absence of Kif5b, a previously described molecular motor regulating myonuclear spreading in myotubes and myofibers[1,9,24,25].

NuMA1 is well known as a key player in cell division, particularly in mitotic spindle orientation[26,27], but no specific role has been described in post-mitotic muscle cells. We next confirmed that efficient si/shRNA-mediated depletion of *Numa1* in either primary mouse myoblasts or immortalized murine myoblasts inhibited myonuclear spreading in both myotubes and myofibers (Fig.2a-i, Supplementary Fig.2a-e). In control condition, quantification of the "mean Distance between Myotubes centroid and Myonuclei" (DMcM) progressively increased as new myonuclei were incorporated into myotubes (Fig.2g), reflecting physiological myonuclei spreading during myotube growth and elongation (Supplementary Fig.2c). In contrast, *Numa1* down-regulation prevented DMcM from increasing, leaving it relatively stables despite the incorporation of new myonuclei. This confirmed a precocious myonuclear aggregation phenotype, preferentially at the myotube center (Fig.2g), and was associated with impaired elongation (Supplementary Fig.2c). We confirmed the specific involvement of NuMA1 in this myonuclei spreading process by rescue experiments using an siRNA-resistant human-NuMA1 construct, which restored proper myonuclei alignment (Supplementary Fig.2f-g). Long-term *Numa1* depletion in myofibers also resulted in persistent myonuclear aggregation, with 40% of myofibers displaying this phenotype compared with only 10% in controls, along with reduced peripheral positioning of myonuclei (Fig.2d-f, h-i). Because myonuclei aggregation in myotubes can also arise from enhanced fusion[14], we assessed the number of myonuclei per myotube (fusion index) in *Numa1* depleted condition or NuMA1 overexpression condition (Supplementary Fig2.h). Unexpectedly, low NuMA1 levels favored myoblast fusion, whereas NuMA1 over-expression slowed down fusion. These findings suggest that NuMA1 abundance also influences myoblast fusion capacity and thereby modulates the timing necessary for proper myonuclear dispersion.

NuMA1 controls myonuclear velocity

We previously demonstrated that myonuclei aggregation correlates with the capacity of myonuclei to move[9,13,14]. To confirm the role of NuMA1 in regulating myonuclear velocity and exclude confounding effects from altered cell fusion, we investigated whether NuMA1 directly controls myonuclear motion. Using time-lapse confocal microscopy, we tracked myonuclei displacement in control (scramble siRNA-treated cells) and *Numa1*-depleted myofibers (Fig.2j-l). In controls, myonuclear motion occurred at a median speed of 0,27 ± 0,01 µm/min, with pauses lasting approximately 2,5 hours per day, resulting in a median daily displacement of

≈350 µm (Fig. 2k-l, supplementary Fig.3a). In contrast, *Numa1* depletion increased pause duration by nearly fourfold and reduced median speed to 0,18 ± 0,01 µm/min, yielding an average daily displacement of only around 100 µm (Fig.2k-l, supplementary Fig.3a). Quantification of myonuclei circularity revealed a nearly 10% increase in *Numa1*-depleted myofibers compared with controls, reflected by rounder myonuclei (Fig.2m, supplementary Fig.3b-c). These data confirm that NuMA1 is involved in myonuclei displacement and suggest that the myonuclei aggregation phenotype upon *Numa1* depletion results from impaired myonuclei spreading in parallel with increased fusion events. To note, myonuclei roundness cannot be considered a direct marker of velocity: while both *mdx* and *Numa1*-depleted myofibers displayed a 10% increase in circularity, the former was associated with enhanced myonuclei displacement (*mdx* myofibers), whereas the latter exhibited severely reduced displacement (*Numa1*-depleted myofibers) (Fig.1-2). Thus, the myonuclei aggregation phenotype is closely associated with modulation of myonuclear velocity.

NuMA1 is a nuclear protein that accumulates into the cytoplasm of myofibers

NuMA1 has been characterized as a nuclear protein that mediates MT-membrane anchoring during mitosis[27]. This MT-related activity is enabled in mitotic cells by the absence of nuclear envelope, which allows NuMA1 to localize to the cytoplasm of mitotic cells; following nuclear envelope reformation, NuMA1 is re-imported and sequestered into the nucleus *via* its Nuclear Localization Sequence (NLS)[28]. To explore the potential mechanisms by which NuMA1 regulates myonuclear motion, we investigated its subcellular localization in muscle cells throughout myogenesis (Fig.3a). As expected, NuMA1 was exclusively nuclear in proliferating murine primary myoblasts (Fig.3b, MyoB) and in human primary myoblasts (Fig.3g, asterisk). Unexpectedly immunofluorescence revealed a progressive accumulation of NuMA1 in the cytoplasm of myotubes, appearing as small puncta, concomitant with a modest increase in its overall mRNA expression during myogenesis (Fig.3b, g, MyoT, Supplementary Fig.3d-f). Quantification of the cytoplasmic NuMA1 signal intensity throughout myogenesis confirmed this progressive accumulation, which also occurred within the myonuclear compartment (Fig.3c-d). In culture conditions promoting “full myofiber maturation” with well-developed sarcomeres and peripherally positioned myonuclei, remaining immature myotubes that failed to achieve this step (iMyoF) exhibited reduced NuMA1 level within myonuclei, suggesting that NuMA1 nuclear localization is dynamically regulated according to the maturation status of myofibers (Fig.3d). To confirm the cytoplasmic accumulation, subcellular fractionation assays were performed on myoblasts and myotubes, and corroborated the immunofluorescence

findings: NuMA1 was exclusively nuclear in proliferative myoblasts, but present in both nuclear and cytoplasmic fractions in myotubes (Fig.3e-f). Similarly, differentiated human primary myoblasts exhibited a progressive cytoplasmic accumulation of NuMA1, confirmed by fractionation analysis (Fig.3g, Supplementary Fig.3g). We next investigated NuMA1 subcellular localization in long-term mature myofibers using *ex-vivo Tibialis Anterior* (TA) myofibers (Fig.3h). Immunostaining revealed predominant nuclear NuMA1, with a cytoplasmic pool capping the extremities of elongated myonuclei. These regions overlapped with MTs and were preferentially situated at microtubule nucleation sites in mature myofibers[29]. Together, these results demonstrate that NuMA1 is exclusively nuclear in proliferating murine and human myoblasts but progressively accumulates in the cytoplasm upon muscle cell differentiation, with distinct spatial enrichment in mature myofibers.

NuMA1 controls the microtubule network thought nuclear-MTOC organization

NuMA1 contains two MT-binding domains that play a crucial role during mitosis, especially for MT nucleation and mitotic spindle orientation[30–33]. As myonuclei alignment in myotubes is mainly mediated by MT interactors[34], we next investigated the role of NuMA1 in maintaining MT network architecture during muscle differentiation (Fig.4). We first examined MT network organization in *Numa1*-depleted myotubes using immunostaining. As expected, depletion resulted in numerous, non-aligned MT intersections compared with the well-ordered arrays observed in scramble conditions (Fig.4a-b). To better identify the cause of this MT disorganization, we analyzed MT plus-end dynamics and orientation using live-cell microscopy of GFP-tagged End-Binding-protein-1 (EB1) in either scramble or *Numa1* siRNA conditions. EB1-GFP comets velocity was unaffected by *Numa1* depletion condition, suggesting that NuMA1 does not regulate MT polymerization rate (Supplementary Fig.4a-b). As we previously observed cytoplasmic NuMA1 adjacent to the myonuclei envelope in mature myofibers (Fig.3h), we next analyzed MT plus-end orientation in two defined regions of myotubes: the "myonuclear zone" and the "nuclear-free zone" (distal tips of myotubes) (Fig.4c). In control condition, MT growing ends orientation are mainly tangential to the longitudinal axis of myotubes, no matter the presence of myonuclei (Fig.4c-g). Interestingly, in *Numa1* depleted conditions, EB1-GFP comets trajectories appears with more randomized orientations in the "myonuclei zone" while the orientation was not affected in the "free myonuclei zone" (Fig.4f-g). This result suggests a specific role of NuMA1 at the vicinity of myonuclei rather than all along myotubes length. In myotubes, MTs mainly emanate from the myonuclei membrane (*i.e.* nMTOC) thanks to the sequential recruitment of several MT nucleator proteins at the membrane

of myonuclei such as AKAP9, Pericentrin and the pericentriolar Material1 (PCM1)[34]. NuMA1 was previously identified as a MT minus-end interactor in mitosis[33]. We thus examined the recruitment of components of the nMTOC throughout the differentiation process in *Numa1*-depleted conditions in both myoblasts and myotubes (Fig.4h-k). In control condition, differentiating myoblasts progressively accumulate at myonuclei membrane PCM1, Pericentrin and Golgi proteins. This process is usually partial in myocytes and fully completed in myotubes, reflected by a 100% coverage of the staining's related to these proteins with the membrane of myonuclei (Fig.4h-k, Supplementary Fig.4c-e). Interestingly, in *Numa1*-depleted conditions, we already observe a failure in the ability of myoblasts to recruit PCM1 at the nuclear membrane but not significant changes in the recruitment of Pericentrin or Golgi proteins (Fig.4h-k, supplementary Fig.4c-e). However, in control myotubes, 100% of myonuclei exhibit PCM1, Pericentrin and Golgi proteins at the vicinity of myonuclei while in *Numa1*-depleted conditions, only 58% of myonuclei present a full recruitment of PCM1, 45% of myonuclei present a full recruitment of Pericentrin and 42% of myonuclei present a full recruitment of Golgi proteins (Fig.4h-k, supplementary Fig.4c-e). These results suggest that cytoplasmic-NuMA1, through the control of proteins recruitment at the nMTOC, constrains MT growth orientation in the longitudinal axis of myotubes. To confirm *in vivo* the key role of NuMA1 in the organization of the microtubules network, we conducted *Numa1* depletion *in vivo* for 2 weeks in the TA muscle of 8 weeks-old mice (Fig.4i-m). Using this approach, we observed a strong alteration of the MT network architecture with an apparent loss of transversally oriented MTs compared to longitudinally oriented MTs observed in control (Fig.4l-n). Altogether our data show that the cytoplasmic NuMA1 in developing myofibers shape the MT patterning through the control of myonuclei-MT anchoring points that contribute to myonuclei displacement and positioning.

NuMA1 accumulation in the nucleus is controlled by AMPKα1 activity

As numerous MAPs, NuMA1 activity is controlled by phosphorylation[35]. Several kinases have been identified targeting NuMA1 to control the mitotic spindle orientation during mitosis such as ABL1, Aurora-A, Plk1 or CDK1[36–38] (supplementary Fig.5a). In a biochemical approach, Schaffer *et al* identified AMPK as a direct target of NuMA1[39] with AMPK phosphorylated site localized on the serine-1853, in the C-terminus part of NuMA1 (Supplementary Fig.5a). AMPK activity in muscle stem cells is mainly assigned to AMPKα1 rather than AMPKα2[40]. To confirm the implication of AMPK in myofiber formation, we thus first investigated myonuclei organization and velocity in primary myotubes using either WT or AMPKα1-KO myotubes

(Fig.5a-c). AMPKα1-KO myotubes exhibit twice less myotubes with aligned myonuclei (Fig.5a-b), unrelated to the alteration in myoblast fusion (Supplementary Fig.5b) showing that AMPK, as NuMA1, is involved in setting MND in developing myotubes (Fig.2). Quantification of myonuclei velocity did not reveal any significant alteration (Supplementary Fig.5c). However, the total distance displacement was enhanced by more than 30%, passing from 110 µm in WT condition to 150 µm in AMPKα1 KO myotubes (Fig. 5c) and was mainly attributed to a decrease in the time myonuclei "pause" in myotubes (Supplementary Fig.5d).

These data show that AMPKα1 activity is required for myonuclei spreading in myotubes and suggest that NuMA1-AMPKα1-related phosphorylation restrain myonuclei displacement, potentially through the maintenance of a cytoplasmic pool of NuMA1 in myotubes. We thus investigated if the absence of AMPKα1 impact nuclear accumulation of NuMA1 in AMPKα1-KO myotubes/myofibers (Fig.5d-i). We first analyzed in AMPKα1-KO myotubes, nuclear NuMA1 content using immunofluorescence approaches (Fig.5d). Quantification of the NuMA1 mean intensity in myonuclei show a 70% increase in AMPKα1-KO myotubes compared to control condition (Fig.5e). To confirm this results, we investigated on the nuclear NuMA1 intensity in myofibers using transverse sections of 2 months-old TA muscle fibers, extracted from either WT or AMPKα1-KO mouse (Fig.5f). Nuclear NuMA1 intensity quantification shows an increase of 30% in AMPKα1 KO myofibers compared to control (Fig. 5h). To avoid technical variations due to the localization of myonuclei in mature myofibers (at the periphery or under the basal lamina), we performed a TA muscle injury step in either WT or AMPKα1 KO mice using cardiotoxin injection that induce a complete muscle regeneration process. In these conditions, after 28 days, all myonuclei remain in the center of myofibers[34,41], allowing a better discrimination of myonuclei (Fig.5g). Quantification of NuMA1 myonuclei intensity show 40% increase in the mean intensity (Fig.5i), confirming that AMPKα1 has a role in the accumulation of NuMA1 in the nuclear compartment. To assess if NuMA1 phosphorylation status is necessary for this preferential accumulation, we overexpressed mutated version of human NuMA1, tagged with GFP and mimicking either a non-phosphorylable version of NuMA1 (with serine-1853 replaced by an alanine) or a phospho-mimetic version of NuMA1 (with serine-1853 replaced by an aspartic acid) (Fig.5j). As expected, the human NuMA1-GFP constructs exhibit a myonuclei staining, with various accumulation of NuMA1 inside myonuclei, suggesting intrinsic variability in the NuMA1 protein uptake by myonuclei according to the phosphorylation status (Fig.5k, Supplementary Fig.5e). Quantification of NuMA1 mean intensity into myonuclei show no differences between NuMA1-WT and the non-phosphorylable version of NuMA1 while it decreases about half in the phospho-mimetic

version of NuMA1 (Fig.5l), confirming that the phosphorylation status affects its ability to be kept by myonuclei. Interestingly, the overexpression of NuMA1 impact the shape of myonuclei that appears smaller, reflected by the myonuclei area (Fig.5m). We next addressed if nuclear NuMA1 content impact myonuclei velocity and displacement into myofibers (Fig.5n-o, Supplementary Fig.5f). Interestingly, we found that accumulation of NuMA1 into myonuclei is correlated with an enhancement in myonuclei speed, whatever the phosphorylation version of NuMA1 (Fig.5n) and lead to an increase in the total distance travelled by each myonuclei, except for the phospho-mimetic version of NuMA1, that pass three more time pausing compare to controls, NuMA1-WT and the non-phosphorylable version of NuMA1 (Fig.5o, Supplementary Fig.5f). These data suggest that nuclear NuMA1 content can potentially reflect the motility of myonuclei and that the AMPK-related phosphorylation of NuMA1 restrain its uptake by myonuclei and block the movement by inducing myonuclei pauses. Finally, to better show that the activity of AMPK controls the ability of myonuclei to uptake NuMA1, we used Benzimidazole derivative small-molecule 991, a known enhancer of AMPK activity[42] and applied it directly onto WT primary myotubes (Fig.5p-q). Our results show that the activation of AMPK leads to the decrease of the mean intensity of NuMA1 inside myonuclei after 1 hour treatment (Fig.5q), suggesting that the myonuclei uptake control of NuMA1 is a dynamic process. Together, our data show that AMPK, through its phosphorylation activity on the serine-1853 of NuMA1, controls its uptake by myonuclei and impacts myonuclei velocity and shape.

NuMA1 is accumulated in dystrophic myonuclei and tunable by drugs targeting AMPK activity

Our finding shows that myonuclei with increased mobility accumulate NuMA1 inside myonuclei (Fig.5) and that *mdx* myonuclei are highly dynamic myonuclei (Fig.1) suggesting a correlation between NuMA1 myonuclei content and their ability to move inside myofibers. To further confirm this hypothesis, we first quantified NuMA1 intensity in myonuclei from 2-months old WT or *mdx* mice, using transversal muscle section of *Soleus* muscle (Fig.6a-b). We showed that *mdx* myofibers exhibit increased NuMA1 myonuclei content (Fig.6b). Interestingly, peripheral myonuclei accumulated less NuMA1 than centralized myonuclei, suggesting different NuMA1 uptake dynamics in peripheral compared to centralized myonuclei (Fig.6b). We confirmed these results using extracted myofibers from *mdx* TA muscle (Fig.6c-d). To explore our results in human pathological context, we next obtained *Quadriceps* biopsies from either control or DMD patient to performed quantification of NuMA1 myonuclei intensity on transversal muscle sections (Fig.6e-g). With this approach, we first observed a strong

heterogeneity in NuMA1 intensity, nevertheless when NuMA1 intensity is plotted according to myonuclei area, we found that in control patients, 72% of myonuclei exhibit a level of NuMA1 that do not excess 2-fold change (with myonuclei area limited to 45 μm^2) (Fig.6f). On the opposite, this category of myonuclei only reach 46% in DMD patients, with some myonuclei that accumulate up to 6-fold NuMA1 in myonuclei with no particular change in myonuclei area distribution (Fig.6g). These data confirm a common pathway in Duchenne myopathy regarding the accumulation of NuMA1 in nuclear compartment and suggest a variability in the motility of myonuclei inside myofibers. Finally, based on our previous finding that activation of AMPK pathway with the Benzimidazole derivative small-molecule 991 inhibited NuMA1 myonuclei accumulation (Fig.5p-q) and the reported ability of AMPK stimulation to enhance muscle function and protect muscle in dystrophic mice[43–45], we next explored whether treatment of *mdx* mice with an AMPK activator would influence nuclear NuMA1 accumulation (Fig.6h-i). We thus evaluated in fibrotic dystrophic mice model[46] the effect of metformin, a known activator of the AMPK pathway[47]. Our results showed that metformin-related activation of AMPK results in a 30% decrease in the mean intensity of NuMA1 inside myonuclei (Fig.6h-i), suggesting that the benefit of metformin treatment in *mdx* mice models could be partly due to its effect on NuMA1 myonuclei shuttling[43]. To better appreciate the direct implication of the AMPK activity effect in *mdx* muscle cells, we next manipulated the activity of AMPK by treating *mdx* myotubes either with a specific activator of AMPK (Benzimidazole derivative small-molecule 991) or with an inhibitor of the AMPK (BAY 3827[48]) (Fig.6j-l). Activation of the AMPK pathway, as expected, decreased the intensity of nuclear NuMA1 while the inhibition dramatically enhanced nuclear NuMA1 (Fig.6j-k). Our finding also showed that AMPK activity restores the capacity of myonuclei to correctly align in developing myofibers (Fig.6l). Interestingly, we did not observe any effect with the activation or inhibition of the AMPK pathway in control conditions while we observed a clear benefit of the AMPK pathway activation in *mdx* myotubes with a 60% increase in the ability of myotubes to correctly align myonuclei (Fig.6l). Our observation thus shows that in dystrophic condition, NuMA1 shuttling between the cytoplasmic compartments and myonuclei is controlled by the AMPK activity and can be pharmacologically modulated with a benefic effect on MND patterning.

Discussion

Myonuclei are located between the plasma membrane of myofibers and myofibril structures[49]. Their peripheral localization induces drastic changes in their shape, primarily due to forces exerted on the nuclear envelope. This conformational adaptation is thought to stabilize both internal and external mechanical forces, and consequently, to influence chromatin organization and gene expression[3,50]. The spatial organization of peripheral myonuclei is determined by the interplay among various cytoskeletal components (microtubule, actin and intermediate filaments). Consequently, myonuclei spatial distribution establishes MND within myofibers, which contribute to the spatial coordination of transcriptomic activity, and, ultimately, to the functional integrity of the myofiber[51]. Accordingly, nuclear spreading at the periphery of muscle fibers is a prerequisite to obtain fully functional mature myofibers[1,2,13]. Myonuclei are considered relatively stable when peripheral, remaining anchored at specific locations along mature mammalian skeletal muscle fibers. However, it is common to observe merged/aggregated myonuclei with various shapes and orientations along mature myofibers, particularly in aged myofibers[16], suggesting that myonuclei possess varying abilities to move within the same myofibers.

Myonuclei motility is a marker of pathological conditions and is linked to the microtubule nucleation at the myonuclei membrane

In this study, we show that the modulation of an optimal myonuclei motion is deleterious for the establishment of MND settings in developing myofibers. Decreasing the ability of myonuclei movement during the first steps of myotubes formation dramatically impaired the initial steps for myonuclei spreading, leading to myonuclei aggregation that counteract the correct establishment of MND settings condition[1,2]. In pathological conditions such as DMD, enhanced myonuclei motility is a precocious event as it can be detected in the first steps of myotubes formation (Fig.1) and persists as a long-term phenotype in *mdx* mice model[52]. Increased myonuclei motility also induces myonuclei aggregation, suggesting that an “optimal” myonuclei motility is needed to set the fundaments of MND in developing myofibers. Interestingly, myonuclei shape (*i.e.* roundness, area) can’t be considered as a motility marker as we observed in *mdx* and *Numa1* depleted myofibers, opposite effects on myonuclei velocity while both conditions increased myonuclei circularity (Fig 1-2). Here, we elucidate the mechanisms by which myofibers control myonuclei motion during muscle fibers formation. Indeed, we demonstrated that the MT binding protein NuMA1 is present at once in the nucleus

and in the cytoplasm in developing myofibers (Fig.3). Cytoplasmic NuMA1 acts on myonuclei motion abilities through the modulation of the cytoskeleton meshwork in the vicinity of myonuclei and controls nMTOC proteins recruitment at the membrane of myonuclei (Fig. 4). Interestingly, this activity is regulated by AMPK phosphorylation, which contributes to restrain NuMA1 inside the cytoplasmic compartment and thus counteracts the capacity of NuMA1 to be taken up by nuclei through its NLS domain, leading to the presence of myonuclei with varying NuMA1 content, correlated with their motility ability (Fig.5). It is tempting to think that in the course of myotubes formation, after fusion events, the various motility of myonuclei observed is dependent on the previously existing NuMA1 content in myoblasts' myonuclei and over time, progressively NuMA1 uptake by myonuclei becomes more homogenous throughout the length of myotubes/myofibers allowing a "myonuclei velocity equilibrium" that favors myonuclei spreading. This hypothesis is supported by the strong differences in myonuclei content between myotubes and myofibers (Fig3.g). Future work should address the status of NuMA1 in myonuclei content during accretion phases, as well as the local activity of AMPK that spatially controls myonuclei spreading.

A key role for NuMA1 in skeletal muscle fibers

In proliferating cells, NuMA1 is a nuclear protein, playing an important role in chromosome decondensation at the mitotic exit[53]. During mitosis, NuMA1 interacts with dynein to reach the poles of mitotic spindle to stabilize and oriente the mitotic spindle[54]. At the end of mitosis, the nuclear envelope is reformed, NuMA1 is then taken up inside the nucleus with its NLS sequence[55]. NuMA1 was initially described to be degraded in post-mitotic muscle cells[56]. In our study, we demonstrated that NuMA1 is well expressed in developing myofibers (Fig.3) and discovered a cytoplasmic role of this protein in the post-mitotic myofibers (Fig.3-5). Indeed, we show that NuMA1 controls nMTOC proteins recruitment at the membrane of myonuclei allowing the correct MT network polymerization orientation inside the developing myofibers to permit MND establishment (Fig. 2-4). NuMA1 was recently identified to have a cytoplasmic role in post-mitotic neurons, in the context of Huntington's disease, also with an impact on the MT network within the growth cones of the axon[57]. Despite the well-documented cytoplasmic role of NuMA1 in mitosis, its nuclear role remains elusive. NuMA1 is a large coiled-coil protein present throughout the nucleus[58] and is nearly as abundant as nuclear lamins, suggesting a major role as a component of the nucleoskeleton[28]. In this view, NuMA1 has the capacity to form long coiled-coiled homodimers that can self-assemble to generate three-dimensional space filling structures[59] likely contributing to nuclear shape. Interestingly, we found that in *Numa1*-depleted

muscle cells, myonuclei circularity is increased in myotubes (Fig.2), and the phosphorylation status also impacts myonuclei conformation (Fig.5). Additionally, NuMA1's involvement in chromatin and nuclear architecture organization is associated with cellular differentiation[60]. As a soft space-filling or matrix protein, NuMA1 could three-dimensionally scaffold other nucleoskeletal structures and consequently mediate genome organization and mechanotransduction[61]. Future work should address the role of NuMA1 in the nucleus compartment, related to transcriptional activity within the muscle cells.

Nuclear mis-positioning and myopathies

Numerous muscles diseases are characterized by alterations of myonuclei shape and myonuclear domain alteration. In DMD, the absence of dystrophin leads to the most frequent form of muscular dystrophy with repetitive degeneration/regeneration cycles that progressively trigger accumulation of damaged myofibers with aberrant myonuclei positioning[62]. Dystrophin is also described as a MAP and accordingly, in DMD animal models, alterations of MT network and myonuclei motion has been observed[20,52,63] and we confirmed this impairment in the present study (Fig.1). Moreover, we demonstrated that nuclear NuMA1 contents are elevated in the *mdx* mouse model and in DMD patients (Fig.6). Our experiments suggest that NuMA1 accumulation in myonuclei could be considered a marker of both myonuclei dynamic within myofibers and alterations in MT network integrity. Interestingly, we demonstrated that modulation of AMPK activity can directly affect nuclear NuMA1 accumulation and influence myonuclei dynamics, with beneficial effects on myonuclear spreading, when pharmacologically activated using a specific AMPK activator, such as the Benzimidazole derivative small-molecule 991 (Fig.6). As AMPK activation has previously been shown to have beneficial effects on muscle function in dystrophic mice[43–45], our work highlights a new positive role for AMPK in muscle regeneration that goes beyond its previously described role in the regulation of inflammation[64–66]. Such actions should be further investigated through the study of NuMA1 muscle-specific activity and extended to other myopathies characterized by myonuclei mispositioning, such as centronuclear myopathies and related diseases[34]. Future work should address how cytoplasmic NuMA1 activity is spatially regulated along muscle fibers and how it contributes to changes in MND in these myopathies. Our findings explain why such diverse phenotypes regarding myonuclei positioning can occur in these myopathies, maintaining aberrant myonuclear localization and, consequently, compromising myofiber integrity.

Figure legends

Figure 1: **Myonuclear dynamics and shape in Duchenne Muscular Dystrophy myofibers**

a. Scheme representation of the experimental procedure for isolating *Tibialis Anterior* myofibers. **b.** Representative immunofluorescence images of isolated *Tibialis Anterior* myofibers from 2-month-old WT or *mdx* mice, stained for MTs (green) and myonuclei (red) (Scale bar: 10 µm). **c/d.** Quantification of the distance between nearest myonuclei (µm) (n=3 independent WT and *mdx* mice, 208 WT and 250 *mdx* measurements) (c) and myonuclei circularity (n=3 independent WT and *mdx* mice, 255 WT and 295 *mdx* myonuclei quantified) (d). **e.** Schematic of the *in vitro* experimental procedure for forming WT or *mdx* primary myotubes after Lamin-RFP-Chromobody® transfection to track myonuclear movements. **f.** Kymograph from 24 h timelapse of 5-day WT or *mdx* primary myofibers transfected with Lamin-RFP-Chromobody®. First frame shows a myofiber; images acquired every 15 min. **g.** Quantification of myonuclear circularity in 3-day WT or *mdx* primary myotubes *in vitro* (n=3 independent primary cultures, 126 WT and 157 *mdx* myonuclei analyzed). **h-i.** Quantification of myonuclear speed (µm/min) (h), and total displacement (µm) (i) in 5-day WT or *mdx* primary myofibers *in vitro* (n=3 independent primary cultures, 300 WT and 239 *mdx* myonuclei tracked). **j.** Quantification of the percentage of myotubes with aligned myonuclei in 3-day WT or *mdx* primary myotubes *in vitro* (n=4 independent primary cultures).

Figure 2: ***Numa1*** **down-regulation affects myonuclei positioning and dynamics during myofiber formation *in vitro*.**

a. Schematic of *in vitro* experimental procedure of 3-day primary myotubes and 10-day primary myofibers after siRNA or shRNA transfection. **b/c.** Representative immunofluorescence images of 3-day primary myotubes transfected with scramble (b) or *Numa1* (c) siRNA, stained for Myosin Heavy Chain (MHC, green) and myonuclei (red) (Scale bar: 10µm). **d-f.** Representative immunofluorescence images of 10-day primary myofibers after scramble (d) or *Numa1* shRNA (e, f) transfection, stained for shRNA plasmid expression (green), actin (red), and nuclei (blue). Arrows indicate non-peripheral myonuclei; asterisks indicate peripheral myonuclei (Scale bar: 10 µm). **g.** Quantification of Mean Distance between Myotubes centroid and Myonuclei (DMcM) in 3-day primary myotubes after scramble or *Numa1* siRNA transfection (n=6 independent primary cultures, 618 scramble shRNA and 687 *Numa1* shRNA distances measured). **h/i.** Quantification of isolated and aggregated myonuclei (n=3

independent primary cultures, 1452 analyzed events in scramble and 2009 in Numa1 knockdown condition) (h) and peripheral myonuclei frequency (n=4 independent primary cultures, 966 quantified events in scramble and 760 in Numa1 knockdown conditions) (i) in 10-day primary myofibers after scramble or *Numa1* shRNA transfection *in vitro*. **j.** Representative kymograph from timelapse imaging of 5-day primary myofibers co-transfection with Lamin-chromobody®-RFP and scramble or *Numa1* siRNA. The first frame of each representative 16h movie shows a myofiber. Myonuclei were tracked for 16h with one image acquired every 20 min. **k-l.** Quantification of the total distance traveled by myonuclei (µm) (k), and myonuclei speed (µm/min) (l) in 5-day primary myofibers after scramble or *Numa1* siRNA transfection *in vitro* (n=2 independent primary cultures, 214 myonuclei tracked in scramble and 173 in *Numa1* siRNA). **m.** Quantification of myonuclei circularity *in* 3-day primary myotubes after scramble or *Numa1* siRNA transfection *in vitro* (n=3 independent primary cultures, 126 myonuclei in scramble condition and 137 in *Numa1* siRNA).

Figure 3: NuMA1 is a cytoplasmic protein in myofiber

a. Schematic of the experimental procedure for *in vitro* formation of 3-day primary myotubes and 10-day primary myofibers. **b.** Representative images of primary myoblasts (MyoB), 3-day primary myotubes (MyoT) and 10-day primary myofibers (MyoF) stained for NuMA1 (red), microtubules or actin (green) *in vitro* (Scale bar: 10 µm). **c/d**. Quantification of cytoplasmic NuMA1 intensity (a.u.) (n=3 independent primary cultures, 114 MyoB, 155 MyoT and 114 MyoF analyzed) (c), and nuclear NuMA1 intensity (a.u.) (n=3 independent primary cultures, 143 MyoB, 184 MyoT and 33 MyoF and 40 iMyoF analyzed) (d). **e/f.** Western-blot after cell fractionation of primary myoblasts (e) and 3-day primary myotubes (f). Membranes probed with NuMA1, tubulin (cytoplasmic control) and histone H3 (nuclear control). **g.** Representative immunofluorescence images of 8- and 16-day human primary myotubes stained for NuMA1 (red), microtubules or NuMA1 (green) and actin (red) *in vitro* (Scale bar: 10 µm). Asterisks mark mononucleated myoblasts. **h.** High-resolution images of isolated myofibers from 2-month-old WT mice stained for NuMA1 (red), microtubules or Pericentrin (green) (Scale bar: 5 µm).

Figure 4: NuMA1 shapes MT network and nMTOC architecture in myofiber

a/b. Representative images of 3-day primary myotubes transfected with scramble (a) or *Numa1* (b) siRNA, stained for myonuclei (red) and microtubules (green) *in vitro* (Scale bar: 10 µm). **c.** Schematic of EB1-GFP comet analysis in 3-day primary myotubes. **d-e.** Representative

maximal Z-projections of EB3-GFP comets in 3-day primary myotubes after scramble (d) or *Numa1* (e) siRNA transfection, where six consecutive frames were overlapped (first three in green, last three in red) (Scale bar: 9 µm). White asterisks indicate comet orientation in control (d-1 & 2) and in *Numa1* knockdown condition (e-3 & 4). **f/g.** Quantification of comet orientation along the myotube axis at tips (n=3 independent primary cultures, 175 analyzed events in scramble, 260 in *Numa1* knockdown) (f), and in myonuclei areas (n=3 independent primary cultures, 284 analyzed events in scramble siRNA-, 376 in *Numa1* siRNA-transfected) (g). Only myotubes with ≥6 myonuclei were analyzed. **h.** Representative images of 3-day primary myotubes after scramble or *Numa1* siRNA transfection, stained for myonuclei (red) and Pericentrin (PCM1, green) *in vitro* (Scale bar: 10 µm)**. i.** Quantification of the percentage of myonuclei with partial or complete Pericentrin relocalization in primary myoblasts and 3-day primary myotubes after scramble or *Numa1* siRNA transfection (n=3 independent primary cultures). **j.** Representative images of 3-day primary myotubes after scramble or *Numa1* siRNA transfection stained for myonuclei (red) and Pericentrin (green) *in vitro* (Scale bar: 10 µm)**. k.** Quantification of the percentage of myonuclei with partial or complete pericentrin relocalization around myonuclei in primary myoblasts and 3-day primary myotubes after scramble or *Numa1* siRNA transfection (n=3 independent primary cultures). **l/m**. Representative images of *Tibialis Anterior* isolated myofibers from 2-month-old WT mice after 2 weeks of scramble (l) or *Numa1* (m) shRNA down-regulation, stained for myonuclei (red) and microtubules (green) (Scale bar: 10 µm). **n.** Microtubule network organization in *Tibialis Anterior* isolated myofibers from 2-month-old WT mice after 2 weeks of scramble or *Numa1* shRNA, analyzed with TeDT software (n=5 mice / condition).

<u>Figure 5</u>: AMPKα1 regulates NuMA1 localization through phosphorylation

a. Representative images of AMPKα1 WT or KO 3-day primary myotubes stained for Myosin Heavy Chain (MHC, green) and nuclei (red) *in vitro* (Scale bar: 50 µm). **b.** Quantification of the percentage of AMPKα1 WT or KO 3-day primary myotubes with aligned myonuclei (n=3 independent primary cultures, 24 mosaic images in WT and 27 in KO). **c.** Quantification of the total distance (µm) traveled by myonuclei in AMPKα1 WT or KO 5-day primary myofibers (n=3 independent WT cultures with 536 myonuclei analyzed and n=4 independent KO primary culture with 505 myonuclei tracked). **d.** Representative images of AMPKα1 WT or KO 3-day primary myotubes, stained for NuMA1 (gray) (Scale bar: 10 µm). **e.** Quantification of nuclear NuMA1 intensity (a.u.) in AMPKα1 WT or KO 3-day primary myotubes (n=3 independent primary cultures, 234 WT and 278 KO myonuclei analyzed). **f.** Representative images of

Tibialis Anterior cross-sections from 2-month-old AMPKα1 WT or KO mice without injury, stained for NuMA1 (red) and laminin⍺2 (green) (Scale bar: 50 µm). **g.** Representative images of *Tibialis Anterior* cross-sections from 2-month-old Pax7-CreER$^{T2/+}$; AMPKα1$^{fl/fl}$ mice 28 days post-injury (dpi) with cardiotoxin, stained for NuMA1 (red) and laminin⍺2 (green) (Scale bar: 50 µm). **h.** Quantification of NuMA1 intensity (a.u.) in myonuclei of uninjured *Tibialis Anterior* cross-sections from 2-month-old AMPKα1 WT or KO mice (n=3 mice/condition, 88 WT myonuclei and 173 KO myonuclei analyzed). **i.** Quantification of NuMA1 intensity (a.u.) in myonuclei of *Tibialis Anterior* cross-sections of 2-month-old Pax7-CreER$^{T2/+}$ (AMPKα-WT) or *Ampka1$^{fl/fl}$*- Pax7-CreER$^{T2/+}$ (AMPKα-KO) mice, 28 days post-injury (dpi) of cardiotoxin injection (130 WT myonuclei and 160 KO myonuclei analyzed). **j.** Scheme of NuMA1-WT protein domains. The second construct corresponds to a non-phosphorylable mutant in which serine-1853 is substituted by alanine (S1853A), while the third corresponds to a phosphomimetic mutant in which serine-1853 is replaced by aspartic acid (S1853D). **k.** Representative images of 3-day primary myotubes transfected with NuMA1-WT, NuMA1-S1853A or NuMA1-S1853D plasmids, stained for plasmid-GFP (gray) (Scale bar: 10 µm). **l.** Quantification of nuclear NuMA1 intensity (a.u.) in 3-day primary myotubes after overexpression of NuMA1-WT, NuMA1-S1853A or NuMA1-S1853D (n=3 independent primary cultures, 142 WT myonuclei, 119 S1853A and 81 S1853D analyzed). **m.** Quantification of myonuclear area (µm^2) in control 3-day primary myotubes or after overexpression of NuMA1-WT, NuMA1-S1853A and NuMA1-S1853D (n=3 independent primary cultures, 281 control myonuclei, 176 WT, 209 S1853A and 124 S1853D analyzed). **n-o.** Quantification of myonuclear speed (µm/min) (n) and total distance traveled by myonuclei (n) in control 5-day primary myofibers or after overexpression of NuMA1-WT, NuMA1-S1853A and NuMA1-S1853D (n=2 independent primary control cultures, 215 myonuclei tracked; n=3 independent primary cultures, 149 WT, 121 S1853A, and 109 S1853D myonuclei tracked). **p.** Representative images of WT 3-day primary myotubes treated with either DMSO or 991, stained for NuMA1 (red) and microtubules (green) (Scale bar: 10 µm). **q.** Quantification of nuclear NuMA1 intensity (a.u.) in WT 3-day primary myotubes treated with either DMSO or 991.

<u>Figure 6</u>: NuMA1 in myonuclei of Duchenne Muscular Dystrophy

a. Representative images of *Soleus* cross-sections from 2-month-old WT or *mdx* mice, stained for NuMA1 (red) and laminin⍺2 (green) (Scale bar: 150 µm). **b.** Quantification of NuMA1 intensity (a.u.) in peripheral and centralized myonuclei of *Soleus* cross-sections from 2-month-

old WT or *mdx* mice (n=3 mice/condition). **c.** Representative immunofluorescence images of isolated *Tibialis Anterior* myofibers from 2-month-old WT or *mdx* mice, stained for microtubules (green) and NuMA1 (red) (Scale bar: 25 µm). **d.** Quantification of NuMA1 intensity (a.u.) in myonuclei of *Tibialis Anterior* isolated myofiber from 2-month-old WT or *mdx* mice (n=3 mice/condition, 188 WT and 295 *mdx* myonuclei analyzed). **e.** Representative images of *quadriceps* cross-sections from control and DMD patient biopsies, stained for NuMA1 (red) and lamininα2 (green) (Scale bar: 150 µm). **f/g**. Quantification of NuMA1 intensity (a.u.) relative to myonuclei area (μm^2) in control (f) or DMD (g) patient biopsies (n=4 control patients,270 analyzed myonuclei for patient 1, 259 for patient 2, 127 for patient 3 and 68 for patient 4. n= 5 DMD patients, 346 analyzed myonuclei for patient 5, 377 for patient 6, 117 for patient 7, 109 for patient 8 and 430 for patient 9). **h.** Representative images of *Tibialis Anterior* cross-sections from 3-month-old *mdx* mice treated or not with metformin, stained for NuMA1 (red) and lamininα2 (green) (Scale bar: 150 µm). **i.** Quantification of NuMA1 intensity (a.u.) in myonuclei of *Tibialis Anterior* cross-sections from 3-month-old *mdx* mice treated or not with metformin (n=5 mice/condition, 545 analyzed myonuclei in untreated *mdx* and 488 after metformin treatment). **j.** Representative images of 3-day *mdx* primary myotubes treated with DMSO, 991 or BAY3827 and stained for NuMA1 (gray) (Scale bar: 10 µm). **k.** Quantification of NuMA1 intensity (a.u.) in myonuclei in 3-day *mdx* primary myotubes treated with DMSO, 991 or BAY3827 (n=3 independent primary cultures, 2029 DMSO, 111 in 991 and 2668 in BAY3827 analyzed myonuclei). **l.** Quantification of the percentage of *mdx* myotubes with aligned myonuclei after DMSO, 991 or BAY3827 treatment (n=4 independent primary cultures for DMSO; n=3 independent primary cultures 991 and BAY3827 treatments).

<u>Supplementary figure 1</u>: Extended duration of *mdx* myonuclei movement and identification of MT-associated proteome involved in myonuclei positioning.

a/b. Quantification of persistence of myonuclei displacement (a.u.) (a) and total pausing time (min) (b) in 5-day WT or *mdx* primary myofibers *in vitro* (n=3 independent primary cultures, 300 WT and 239 *mdx* myonuclei tracked). **c.** Schematic of the biochemical procedure for purification and identification of proteins involved in myonuclei positioning in 3-day primary myotubes and 10-day primary myofibers *in vitro*. **d.** Distribution of partners identified by mass spectrometry; specific to 3-day myotubes, 10-day myofibers, or shared between both. **e.** Quantification of myonuclei spreading index of identified partners in 3-day myotubes, 10-day myofibers, or shared conditions *in vitro*.

Supplementary figure 2: NuMA1 controls myonuclei positioning and myoblast fusion

a. Western-blot showing *Numa1* down-regulation in 3-day primary myotubes after scramble or *Numa1* siRNA transfection and rescue transfection with hNuMA1-GFP plasmid *in vitro*. **b.** Relative *Numa1* mRNA expression in 3-day primary myotubes after scramble or *Numa1* siRNA transfection. **c.** Quantification of myotubes length (µm) in 3-day primary myotubes after scramble or *Numa1* siRNA transfection, classified by myonuclei number per myotube (n=6 independent primary cultures, 618 scramble and 687 *Numa1* siRNA myotubes analyzed). **d.** Representative images of 3-day primary myotubes after scramble or *Numa1* siRNA transfection, stained for Myosin Heavy Chain (MHC, green) and nuclei (red) (Scale bar: 50 µm). **e.** Quantification of the percentage of 3-day primary myotubes with aggregated myonuclei after scramble or *Numa1* siRNA transfection (n=3 independent primary cultures). **f.** Representative images of 3-day primary myotubes after scramble, *Numa1* siRNA or rescue condition (*Numa1* siRNA + hNuMA1-GFP), stained for MHC (red) and nuclei or hNuMA1-GFP (green) (Scale bar: 50 µm). **g/h.** Quantification of percentage of 3-day primary myotubes with aligned myonuclei (g) and fusion index (h) after scramble, *Numa1* siRNA, or rescue transfection (n=3 independent primary cultures).

Supplementary figure 3: Increased myonuclei pause duration and altered shape upon *Numa1* down-regulation

a. Quantification of total myonuclei pausing time (min) in 5-day primary myofibers after scramble or *Numa1* siRNA transfection (n=2 independent primary cultures, 214 scramble and 196 *Numa1* siRNa myonuclei tracked). **b/c.** Representative immunofluorescence images of 3-day primary myotubes after scramble (b) or *Numa1* (c) siRNA transfection, stained for myonuclei (gray) (Scale bar: 15 µm). **d-e.** Relative expression of *Numa1* (d) and *Myosin Heavy Chain 4* (e) mRNA during C2C12 differentiation (n=3 independent cultures). **f.** *Numa1* and *Myosin Heavy Chain 4* mRNA relative expression in 3-day primary myotubes and 10-day primary myofibers (n=3 independent primary cultures). **g.** Western-blot of 5-day human primary myotubes cell fractionation, probed for NuMA1; HSP90 and histone H3 used as cytoplasmic and nuclear loading controls, respectively.

Supplementary figure 4: NuMA1 in MT polymerization and nuclear MTOC organization

a. Representative timelapse images of 3-day primary myotubes co-transfected with EB1-GFP and either scramble or *Numa1* siRNA *in vitro* (Scale bar: 9 µm). **b.** Quantification of EB1-GFP

comet velocity (µm/min) in 3-day primary myotubes with scramble or *Numa1* siRNA transfection (n=3 independent primary cultures, 1183 scramble and 2154 in *Numa1* siRNA comets tracked). **c/d**. Representative images of 3-day primary myotubes after scramble (c) or *Numa1* (d) siRNA transfection, stained for myonuclei (red) and GM130 (green) (Scale bar: 10µm)**. e.** Quantification of the percentage of myonuclei with partial or complete GM130 relocalization around myonuclei in primary myocytes or 3-day primary myotubes after scramble or *Numa1* siRNA transfection (n=3 independent primary cultures).

<u>Supplementary figure 5</u>: Nuclear NuMA1 content drives myonuclei dynamics

a. Schematic of NuMA1 protein domains highlighting phosphorylation sites targeted by kinases. **b.** Quantification of fusion percentage in 3-day *Ampka1* WT or KO primary myotubes (n=3 independent primary cultures, 15 mosaic images analyzed). **c/d.** Quantification of myonuclei speed (µm/min) (c) and total pausing time (min) in 5-day *Ampka1* WT or KO primary myofibers (n=3 independent WT primary cultures with 536 analyzed myonuclei and n=4 independent KO primary cultures with 505 myonuclei tracked). **e.** Representative images of 3-day primary myotubes after hNuMA1-WT transfection, stained for plasmid-GFP (green) and myonuclei (red) (Scale bar: 10 µm) **f.** Quantification of myonuclei total pausing time (min) in 3-day primary myotubes in control or transfected with NuMA1-WT, NuMA1-S1853A, or NuMA1 S1853D (n=2 independent primary cultures for control, 215 myonuclei tracked ; n=3 independent primary cultures for mutants, 149 WT, 121 S1853A, and 109 S1853D myonuclei tracked).

706

707 Materials and methods

708 Reagents

siRNA	Sense oligonucleotide sequence	Anti-Sense oligonucleotide sequence
Scramble	Ambion, AM4641	
Numa1	GGGCAAGGUGAAGCAUUAA	UAAUGCUUCACCUUGCCC

709

shRNA	Clone Name	Target sequence
Scramble	SHC002 (MERCK)	Non target sequence
Numa1	TRCN000007230 (Sigma)	GCCAGATGGATCGAAAGATTA

710

Plasmids	
EB1-GFP	From Edgar Gomes' lab (institut myology, Paris, France)
RFP-Lamin-chromobody®	Chromoteck (lcg)
hNuMA1-WT-GFP	From Andreas Merdes' lab (Centre de Biologie Intégrative, Toulouse, France)
hNuMA1-S1853A-GFP	Directed mutagenesis performed in the lab
hNuMA1-S1853D-GFP	Directed mutagenesis performed in the lab

711

712- **Antibody used for cell culture immunostaining**

Antibody	**Species and utility**	**Dilution factor**	**Manufacturer and reference**
α-Tubulin (microtubules)	Mouse – Primary	1/500	Sigma T6074
Myosin Heavy Chain (MHC)	Mouse – Primary	1/10	DSHB
Actin	Mouse – Primary	1/500	Millipore – Mab1501
NuMA1	Rabbit – Primary	1/500	Abcam – EP3976
GM130	Mouse - Primary	1/100	BD Biosciences 610823
PCM1	Rabbit – Primary	1/500	Sigma - HPA023370

Pericentrin	Mouse - Primary	1/100	BD Biosciences 611815
α-Actinin	Mouse - Primary	1/500	Sigma – A7811
Anti-Mouse Alexa Fluor A488	Goat - Secondary	1/1000	Thermofisher scientific – A-11029
Anti-Rabbit Alexa Fluor A555	Goat - Secondary	1/1000	Thermofisher scientific – A-21428
DAPI (nuclei/myonuclei)	Dye	1/5000	Thermofisher scientific D1306

713

714- **Antibody used for isolated myofibers**

Antibody	**Species and utility**	**Dilution factor**	**Manufacturer and reference**
DAPI (myonuclei)	Dye	1/5000	Thermofisher scientific D1306
NuMA1	Rabbit – Primary	1/500	Abcam – EP3976
Tyrosinated Tubulin (Microtubules)	Rat – Primary	1/500	Andrieux'lab
Pericentrin	Mouse - Primary	1/100	BD Biosciences 611815
Anti-Mouse Alexa Fluor A488	Goat - Secondary	1/500	Thermofisher scientific – A-11029
Anti-Rabbit Alexa Fluor A555	Goat - Secondary	1/500	Thermofisher scientific – A-21428

715

716-

717-

718-

719- **Antibody used for muscle transversal cross-section**

Antibody	**Species and utility**	**Dilution factor**	**Manufacturer and reference**
Laminin⍺2	Rat - Primary	1/1000	Santa Cruz – sc-59854
NuMA1	Rabbit – Primary	1/500	Abcam – EP3976
Anti-Rat Alexa Fluor A488	Goat - Secondary	1/500	Thermofisher scientific – A-11006
Anti-Rabbit Alexa Fluor A555	Goat - Secondary	1/500	Thermofisher scientific – A-21428

720

721- **Antibody used for western-blot**

Antibody (WB)	**Species and utility**	**Dilution factor**	**Manufacturer and reference**
⍺-Tubulin	Mouse – Primary	1/1000	Sigma T6074
Actin	Mouse – Primary	1/1000	Millipore – Mab1501
NuMA1	Rabbit – Primary	1/1000	Abcam – EP3976
HSP90	Mouse – Primary	1/1000	Enzo life SPA830
Histone H3	Rabbit – Primary	1/1000	Cell signaling – 9715S
Anti-Mouse HRP	Goat - Secondary	1/5000	Invitrogen 65-6520
Anti-Rabbit HRP	Goat - Secondary	1/5000	Invitrogen 65-6120

722

723- **Primers forward (F) and reverse (R) for qPCR**

Primers	**Sequence**
NuMA1 F	AAGTATTGACAGCCTGGATCTGA
NuMA1 R	GGTACGAGGCAGCTTGCT
GAPDH F	AACTTTGGCATTGTGGAAGG
GAPDH R	ACACATTGGGGGTAGGAACA
MHY4 F	CAAGTCATCGGTGTTTGTGG
MYH4 R	TGICGTACTIGGGAGGGTTC

Gusβ F	GAGGATTGCCAACGAAACCG
Gusβ R	GTGTCTGGGGACCACCTTTGA
RPL41 F	GCCATGAGAGCGAAGTGG
RPL41 R	CICCTGCAGGCGTCGTAG

Primers for directed mutagenesis

NuMA1-S1853A	Forward	CTAGAGACTGAGTAGCGGAGGTGGCTCGCAG
	Reverse	CTGCGAGCCACCTCCGCTACTCAGTCTCTAG
NuMA1-S1853D	Forward	AGCTAGAGACTGAGTATCGGAGGTGGCTCGCAGG
	Reverse	CCTGCGAGCCACCTCCGATACTCAGTCTCTAGCT

Animals and animal experiments

2 months-old male DMD^{mdx4Cv} mice (*mdx*)[67] with C57BL/6 background were used. As a control WT mice, we used C57BL/6 2 months old mice. 3 months-old male *mdx* mice were treated with metformin (Sigma). Metformin was added to the drinking water for 3 weeks (200mg/kg/day, *i.e.* 1mg/ml replaced every day). The 2 first weeks of treatment was concomitant with fibrosis establishment in the fib-mdx model[46]. AMPKα1 WT or KO pups were used to performed primary culture experiment. Heterozygous animals were bred and AMPKα1 pups were genotyping, and myoblasts cells were plate dependent of the genotype of interest WT or KO. 2 months-old adult AMPKα1 WT or KO were used in uninjured condition. For muscle injury experiment, 2 months-old males, Pax7-CreER$^{T2/+}$; AMPKα1$^{fl/fl}$ were used[40]. CreER^{T2} was activated by 2mg/mouse tamoxifen (MP Biochemical – 02156738-CF) injection during 4 consecutives days, 1 week before muscle injury. To performed skeletal muscle injury, intramuscular cardiotoxin (Latoxan, L8102-1MG) injection was performed in *Tibialis Anterior* of mice. Mice were anesthetized with isoflurane inhalation and 50 µl of cardiotoxin were injected. 1x PBS as injected in control mice. Muscles were harvested 28 days post-injury.
All animal experimentations were approved by the French and European legislation. At the end of the procedure, mice were euthanized by an excess of isoflurane inhalation followed by cervical dislocation.

Cell culture

Primary murine cells

Primary mouse myoblasts were purified from wild type C57BL6 newborn mice as described before[19]. Hindlimb muscles from 4 to 7 days pups were extracted and digested with Collagenase

I (Sigma, C9263-1G) and Dispase II (Roche, 04942078001). After 4h of pre-plating to discard contaminant cells such as fibroblasts, myoblasts were cultured on 1% growth factor reduced Matrigel®/IMDM coated-dish (Corning, 356231; Ibidi µ-dish 35mm high ibiTreat, 81256 or µ-Slide 4 Well ibiTreat, 80426) in growth media (IMDM (Gibco, 21980065), 20% fetal bovine serum (Gibco, A5256701), 1% chicken embryo extract (USBiological, C3999), 1% penicillin-streptomycin (Gibco, 15140-122), 0,5% gentamycin and 5% fibroblasts growth factor 2 (Milteny Biotec, 130-105-786)). Myoblasts were induced to differentiate in myotubes when they reached 80% of confluence for 2 or 3 days in differentiation media (IMDM (Gibco, 21980065), 2% horse serum (Gibco, 16050-22) and 1% penicillin-streptomycin (Gibco, 15140-122)). Myotubes were then covered by a layer of 50% growth factor reduced Matrigel®/IMDM (Corning, 356231) and maintain in culture up to 10 days in long differentiation culture media (IMDM (Gibco, 21980065), 2% horse serum (Gibco, 16050-22), 1% penicillin-streptomycin (Gibco, 15140-122) and 0,1% Agrin) until the formation of mature and contracting myofibres. Half of medium volume was changed every two days.

Primary human cells culture for immunofluorescence

Human primary myoblasts were isolated from uninjured semitendinosus muscles collected as surgical waste (protocol CCER no. PB_2016-01793 approved by the Swiss Regulatory Health Authorities and sanctioned by the "Commission Cantonale d'Ethique de la Recherche" of the Geneva Cantonal Authorities, Switzerland). Myoblasts were purified and cultured as described earlier[68]. Cells were seeded on a NanoSurface dish (ANFS-1, NanoSurface Biomedical, Inc.) coated with Matrigel (BD, diluted 1/100 in Ham's F-10, ThermoFisher). After four days of differentiation, a second layer of Matrigel (BD, diluted 1/3 in differentiation medium) was added to cover the myotubes[69]. Half of the medium was replaced every other day.

Primary human cells culture for cell fractionation

Primary human myoblasts were plated on 1% Matrigel-coated dishes and cultured in a proliferative medium containing 40% skeletal muscle cell growth medium with supplemented mix (Promocell, C-23060), 30% DMEM high glucose and pyruvate (Gibco, 41966029), 20% decomplemented FBS (Gibco, 10270-106), 9% medium 100 GlutaMAX supplement (Gibco, 41150-020), 1% penicillin-streptomycin (Gibco, 15140-122), 0,005% Puromycin and 0,003% dexamethasone. Differentiation was induced by a switch into differentiation media (skeletal

muscle cell growth medium, Promocell, C-23060). Differentiation medium was changed every other day.

C2C12 immortalized cells

Mouse myoblasts C2C12 cells were cultured in Dulbecco's modified Eagle's medium (DMEM (Gibco, 41966029) + 15% fetal bovine serum (Gibco, 10270-106) + 1% penicillin-streptomycin (Gibco, 15140-122)) and were plated on 1% matrigel-coated dishes for 1-2 days before induction of differentiation by a switching into differentiation media (DMEM + 1% horse serum).

Cell transfection

Primary myoblast cells were transfected with either Lipofectamine 2000 (ThermoFisher Scientifics, 11668-019) for siRNA transfection at the final concentration of 10 nM, or with Lipofectamine 3000 (ThermoFisher Scientifics, 11668-019) for overexpression plasmids or shRNA transfection at the final concentration of 750 ng/µl, in accordance with manufacturer instructions, just before differentiation. Co-transfection experiments (*i.e.* plasmids and siRNA) were performed using Lipofectamine 2000 (ThermoFisher Scientifics, 11668-019) in accordance with manufacturer instructions.

AMPK pathway activation and inhibition

3-days WT primary myotubes were treated with ADaM-site binding small molecules (991, Selleckcehm – S8654), an allosteric AMPK activator. 10 µM of 991 was added in differentiation medium for 1h at 37°C and cells were fixed. 3-days mdx primary myotubes were treated either with DMSO, 10 µM of 991 or 1 µM of BAY3827 (AMPK inhibitor), for 1h to measure nuclear NuMA1 content or for 24h to see the effect on myonuclei positioning.

Purification of Microtubule-Associated protein

We purified Microtubule-Associated Proteins (MAPs) from 3-days differentiated mouse primary myotubes or 10-days differentiated mouse primary myofibers as described before[70]. Myotubes or myofibers were detached using trypsin/EDTA 1X (Thermofisher scientific 15400054). Cell pellet was diluted in an optimal volume of cold PEM[71] (0,5M of PIPES pH 6.8, 2M of MgCl2, 0.5M EGTA). Cells were sonicated, kept 10 min on ice and lysate were homogenized using QIAshredder (Qiagen, 79656) before being clarified using centrifugation at 45000 rpm with Bockman rotor TLA100.3, at 4°C. To link MAPs and molecular motor to

the MT network, clarified extract was put at 37°C in a water bath and MTs were stabilized with Taxol (Molecular Probes, Cat. No. P-3456). 1 mM of GTP and 1.5 mM of AMP-PNP (adenylyl-imidophosphate) were added to the suspension for 90 min at 37°C in a water bath. Solution of MTs and cell extracts were then put on 40% of glycerol cushion with 10 µm of Taxol diluted in PEM, centrifuged at 45000 rpm for 20 min at 37°C. For 3 times, MTs, MAPs and molecular motors were diluted in appropriate volume of wormed PEM and centrifuged at 45000 rpm, 10min at 37°C. The final pellet was resuspended in water with Bolt reducing agent (Thermofisher scientific, B0009) and Bolt LDS Buffer (Thermofisher scientific, B0007). Spectrometry analysis was performed on a single mix of 3 experiments for each time point (3 days, myotubes and 10 days, myofibers).

Mass spectrometry

Proteins were solubilized in Laemmli buffer and stacked in the top of a 4-12% NuPAGE gel (Invitrogen). After staining with Coomassie blue R-250 (Bio-Rad), they were digested in-gel using modified trypsin (Promega, sequencing grade) as previously described[72]. The resulting peptides were analyzed by online nanoliquid chromatography coupled to MS/MS (Ultimate 3000 and LTQ-Orbitrap Velos Pro, Thermo Scientific). For this purpose, the peptides were sampled on a precolumn (300 µm x 5 mm PepMap C18, Thermo Scientific) and separated in a 75 µm x 250 mm C18 column (PepMap, 3 µm, Thermo Scientific) using a 120-min acetonitrile gradient. The MS and MS/MS data were acquired using Xcalibur (Thermo Fisher Scientific).
Peptides and proteins were identified by Mascot (version 3.1.0, Matrix Science) through concomitant searches against the Uniprot database (*Mus musculus* taxonomy) and a homemade database of contaminant proteins classically found in proteomic analyses (human keratins, porcine trypsin, bovine albumin...). Trypsin/P was chosen as the enzyme and two missed cleavages were allowed. Precursor and fragment mass error tolerances were set at respectively at 10 ppm and 0.6 Da. Peptide modifications allowed during the search were: Carbamidomethyl (C, fixed), Acetyl (Protein N-term, variable) and Oxidation (M, variable). The Proline software[73] (version 2.3.3) was used for the compilation, grouping, and filtering of the results (conservation of rank 1 peptides, peptide length ≥ 6 amino acids, false discovery rate of peptide-spectrum-match identifications < 1%[74], and minimum of one specific peptide per identified protein group). Proline was then used to perform a weighted spectral counting (WSC)-based comparison of the samples. Proteins were considered enriched in a sample compared to another if they were identified by at least 3 WSC and identified only in one sample or enriched at least 5 times in a sample compared to the other on the basis of WSC.

siRNA screening

As described before, primary mouse myoblasts were cultured on 1% growth factor reduced Matrigel®/IMDM coated 96 wells plate (UGAP, 2582249). Cells were transfected with Lipofectamine 2000 (ThermoFisher Scientifics, 11668-019). For each condition, 3 siRNAs are mixed at the final concentration of 10 nM in accordance with manufacturer instructions. Primary myoblasts were put in differentiation media for 3 days before fixation in 4% PFA (Thermoscientific 043368.9M)/ 4% sucrose (Acros organics 177140010) in PBS for 20 min at 37°C and immunofluorescence protocol followed.

Immunofluorescence

- **On primary cells**

Cells were fixed in 4% paraformaldehyde (Thermoscientific 043368.9M) – 4% sucrose (Acros organics 177140010) – 0,1% TritonX-100 in PBS for 20 min at 37°C followed by washes with PBS and membranes permeabilization with 0.5% Triton-X100 in PBS for 5 min at Room Temperature (RT). Following washes with PBS, cells were saturated with 1% BSA in PBS for 30 min at RT and incubated in primary antibodies overnight at 4°C. Following washes with 0.05% Triton-X100 in PBS, cells were incubated in secondary antibodies or dyes for 1h at RT followed by washes with 0.05% Triton-X100 in PBS and a last wash in PBS.

- **On isolated myofibers**

Following dissection of the whole muscle from the mice, *Tibialis Anterior* muscles were fixed in 4% PFA (Thermoscientific 043368.9M)/ 4% sucrose (Acros organics 177140010) in PBS for 2h at RT. After washes, mono-myofibers were isolated from each muscle for each condition. Myofibers were permeabilized using 1% Triton-X100 in PBS for 15 min at 37°C and saturated in 1% BSA in PBS for 30 min at RT. Myofibers were then incubated in primary antibodies at 4°C for 2 nights. Following 0.05% Triton-X100 in PBS washes, myofibers were incubated in secondary antibodies or dyes overnight at 4°C. Then, washes with 0.05% Triton-X100 in PBS and a last wash in PBS were carried. Myofibers were mounted on slides using Fluromount Aqueous mounting (Sigma, F4680) and kept at 4°C.

- **On isolated muscle transversal cross-section**

Tibialis Anterior, muscles were collected, embedded in tragacanth gum, and quickly frozen in isopentane cooled in liquid nitrogen. Cross-sections (10µm thick) were obtained from the middle portion of frozen muscles and processed for immunostaining. Muscle sections were

fixed using 4% PFA (Thermoscientific 043368.9M) and 4% Sucrose (Acros organics 177140010) for 10 min at RT. After several PBS washes, permeabilization step was carried out using Triton X-100 0,1% for 10 min at RT. Sections were saturated in BSA 1% (Euromedex 04-100-812) for 1h at RT. Primary antibodies were incubated overnight at 4°C. The day after sections are incubated with secondary antibodies for 1h at RT following by DAPI for 5 min. Sections were mounted on slides using Fluromount Aqueous mounting (Sigma, F4680) and kept at 4°C.

Images acquisition and analysis

Video microscopy, myonuclei and EB1 tracking

Myonuclei tracking: timelapse images were acquired every 20 or 15 min, using Z1-AxioObserver (Zeiss) or Nikon AX confocal microscope (Nikon), 20X objective. Myonuclei were manually tracked using Metamorph (Zeiss) or Icy software respectively and analyzed using SkyPad® plugin as described before[75].

EB1 tracking: timelapse images were acquired every 150 milliseconds using Ti Eclipse (Nikon) microscope 60X oil objective, Plan Apo, NA: 1.4, WD: 0.13, coverglass thickness: 0.17. EB1 comets trajectory were extracted using ImageJ®. To determine EB1 comets orientation, six continuous frames of a time-lapse movie of EB1-GFP were overlapped, the first three are color-coded in green and the last three are color-coded in red. EB1 comets velocity was measured using Particle Tracker in ImageJ®[76]

High resolution microscopy (SIM)

Following dissection of the whole muscle from the mice, *Tibialis Anterior* muscles were fixed in 4% PFA (Thermoscientific 043368.9M)/ 4% sucrose (Acros organics 177140010) in PBS for 2h at RT. After washes, mono-myofibers were isolated from each muscle for each condition. Heat-induced epitope retrieval was done with steaming method in Antigen Unmasking Solution, Tris-Based (H-3301), 20min. After PBS washes, a blocking step was performed with saturation solution (1X PBS, 0.05% Triton-X100, 3% Bovine Serum Albumin, 5% Normal Goat Serum) for 45 min at RT. Myofibers were then incubated with primary antibodies diluted in saturation solution at 4°C for 4 nights. Following 0.05% Triton-X100 in PBS washes, myofibers were incubated with secondary antibodies overnight at 4°C. Then, washes with 0.05% Triton-X100 in PBS and a last wash in PBS were carried. Myofibers were deposited on

25 mm coverslip 1.5H (Marienfeld, ref:0117650) coated with 5 mg/mL gelatin from bovine skin and 1 mM chromium (III) potassium sulfate to ensure fibers were positioned near the objective to minimize surface irregularities that could compromise resolution. Coverslips were then mounted with Prolong Glass (Fisher ref 15810993).

3D Lattice-SIM images were acquired on a Zeiss Elyra 7 AxioObserver microscope equipped with a Plan-Apochromat 63×/1.46 oil objective and a Photonlines pco.edge 4.2 sCMOS camera and controlled by the software Zen 3.0 SR Black. For fluorescence signal detection, 405 nm (100 mW), 488 nm (100 mW), 561 nm (100 mW) and 640 nm (500 mW) laser lines were used respectively with the filters (nm) BP 420-480_LP 650/ BP 420-480_495-525_LP 650 / BP 495-550_570-620/ BP 420-480_LP 650. 3D Lattice-SIM acquisitions were performed using 13 pattern translations. Z-stacks were acquired using 100 nm intervals. The raw image obtained has a pixel size of 62.61 nm and post processing image has a pixel size of 31.3 nm. Exposure time and laser power were balanced for each fluorescence channel individually to minimize bleaching and exposure time. 3D Lattice-SIM processings were performed using the SIM processing tool from the Zen 3.0 SR Black software.

Confocal microscopy

Isolated myofibers, muscle transversal cross-section and primary cells images were acquired using Z1-AxioObserver (Zeiss) or LSM 880 confocal microscope (Zeiss) or Nickon AX microscope (Nikon) with 60X oil objective.

- **Image analysis**

Myonuclei spreading analysis in myotubes: Quantifications in immature myotubes were assessed using an analysis tool developed in our team. An image analysis performed in ImageJ® software is combined with a statistical analysis in RStudio® software. This provides quantifications of parameters, ranked by myonuclei content per myotubes, regarding phenotype of myotubes (area, length) and their respective myonuclei positioning compared to centroid of myotubes (DMcM). MSG diagrams were obtained through the normalization of lengths of all analyzed myotubes (independently to their myonuclei content) to 100%. White lines represent myonuclei density curves assessing the statistical frequency for myonuclei positioning along myotubes. Each color group reflects statistical estimation of myonuclei clustering along myotubes.

Myonuclei shape, MND organization and NuMA1 intensity: Myonuclei shape was analyzed using Fiji® software. Myonuclei were segmented based on nuclei staining (DAPI) and myonuclei circularity, area, nuclear NuMA1 intensity parameters were extracted. MND organization was analyzed using Fiji® software by measuring the distance between closest myonuclei.

Myonuclei localization in primary myotubes/myofibers: We considered as a 3-days primary myotubes, each structure MHC positive that contain at least 6 myonuclei. In each individual myotube, we considered aligned myonuclei when 70% of myonuclei are well aligned in the center of myotube length. The percentage of myotubes with aligned or aggregated myonuclei was calculated based on the total number of myotubes in the picture.

We considered as 10-days primary myofibers, each structure that contain striated actin staining. The percentage of events with isolated and centralized myonuclei, aggregated or peripherized myonuclei was calculated.

Fusion index: The fusion index was determined by the ratio of the number of myonuclei in MHC positive structure (ie. 3-days primary myotubes) on the total number of nuclei in the picture.

MT architecture organization: MT architecture organization was analyzed using TeDT software as previously described[77].

Statistical analysis

The statistical analyses were performed using Student's t test according to samples amount and distribution.

Protein sample preparation from cell culture

Cells were harvested using trypsin (Gibco, 15400054) for 5 min at 37°C and centrifuged at 1500 rpm for 5 min at 4°C. Cell pellets were diluted and incubated in the optimal volume of RIPA lysis buffer (homemade), containing phosphatase inhibitors (Sigma, P5726) and protease inhibitors (Sigma, P8340), for 10 min at 4°C. Following a sonication step at 4°C, protein samples were collected for further uses. The concentration of proteins was determined using BCA protein assay kit (Thermo Fisher Scientifics, 23225) as described by the manufacturer.

Subcellular fractionation assays from cell culture

Cells were harvested, using trypsin for 5 min at 37°C and centrifuged at 1500 rpm for 5 min at 4°C. Cell pellet was diluted on E1 lysing buffer (NaCl 140 mM, glycerol 10%, NP40 0.5%,

Triton X-100 0.25%, DTT 1mM, EDTA 1mM, Hepes-KOH pH7.5 500mM, phosphatase inhibitors (Sigma, P5726) and protease inhibitors (Sigma, P8340)). After a centrifugation step of 10 min at 5000 g, supernatant containing cytoplasmic fraction was collected in a new tube. Pellet was diluted on the same volume of E1 buffer as mentioned before and centrifuged for 10 min at 5000 g at 4°C. This step was repeated with an additional step of 10 min on ice before the centrifugation and removing supernatant. Pellet was diluted on SDC buffer (NaCl 600 mM, NP40 1%, SDS 0.1%, Tris-HCl pH7.5 50mM, sodium deoxycholate 0.5%, phosphatase inhibitors (Sigma, P5726) and protease inhibitors (Sigma, P8340) following by a sonication step at 4°C, samples were incubated for 30 min on ice, corresponding to the nuclear fraction. All fractions were centrifuged at 10 000 g for 10 min at 4°C and protein samples were collected for further uses.

Western blot

Samples were loaded onto 6% acrylamide gels and migrated at 100V for 10 min followed by 90 min at 130V. Wet blotting system (BioRad) was used to transfer proteins to PVDF membranes (Millipore, Immobilon-P, IPVH00010). Membranes were then saturated in 5% BSA in 0.1% Tween20 – 1X TBS for 1h at RT and were incubated in primary antibodies in 5% BSA in TBS overnight at 4°C. Following washes by 0.1% Tween20 – 1X TBS, membranes were incubated in HRP conjugated secondary antibodies in 1% BSA in TBST for 1h at RT. Following washes in 0.1% Tween20 – 1X TBS, detections of target proteins were carried out using clarity Western ECL substrate (BioRad, 1705060) and ChemiDoc imaging system (BioRad).

RNA extraction from cell culture

After addition of Trizol (Sigma, T9424), samples were incubated in chloroform for 5 min at RT, centrifuged for 15 min at 12000 g at 4°C and incubated in tubes containing isopropanol for 10 min at RT. Samples were then centrifuge for 15 min at 12000 g at 4°C, washed two times with 70% ethanol and RNA pellets were diluted into ultra-pure RNase free water (Invitrogen, 10977-035). RNA concentration was analyzed using Nanodrop® (ThermoFisher Scientifics).

RT-q-PCR

Goscript Reverse Transcriptase System (Promega, A5001) was used as described by the manufacturer to produce the cDNAs. Fast Start Universal SYBR Green Master (Rox) (Roche, 04913914001) and CFX Connect™ Real-Time PCR Detection System (BioRad) were used to

carry out quantitative PCR using primer described in table below. Normalization was performed using housekeeping genes.

Mice electroporation

8 weeks old male C57BL/6 WT mice were anesthetized with intraperitoneal injection of ketamin (100 mg/kg) - xylazin (10 mg/kg). Hind legs were shaved and 20 µg of plasmid DNA diluted into 0.9% NaCl were injected in both contralateral *Tibialis Anterior* muscles. Injected muscles received a short massage, and a thin layer of ultrasound gel was applied. Electrodes were positioned on both side of muscles and an electrical field was applied characterized by 8 pulses of 20 ms spaced 500 ms apart, at 200 V/cm of thickness of muscle (*i.e.* 80 V). Two weeks post-electroporation, mice were sacrificed, and muscles were harvested. The whole experiment procedure is in accordance with the guidelines of the local animal ethics committee of the University Claude Bernard – Lyon 1 and in accordance with French and European legislation on animal experimentation and approved by the ethics committee CECCAPP and the French ministry of research.

Mutagenesis

Directed mutagenesis was performed to introduce punctual mutation in NuMA1-WT plasmid. It was performed following manufacturer instruction with QuickChange II XL site-directed Mutagenesis Kit (Agilent, 200521).

Graphical representation

Graphical boxes showed the higher and the lower point of the population. The median is represented. T-Test were performed to compared the 2 groups.

Funding

This work was funded by grants from ATIP-AVENIR Program, Association Française contre les Myopathies (MyoNeurAlp Alliance) and the ANR NuCytAct (ANR-23-CE14-0078). Proteomic experiments were partially supported by Agence Nationale de la Recherche under projects ProFI (Proteomics French Infrastructure, ANR-10-INBS-08) and GRAL, a program

from the Chemistry Biology Health (CBH) Graduate School of University Grenoble Alpes (ANR-17-EURE-0003).

Acknowledgements

We acknowledge the contributions of the CELPHEDIA Infrastructure (http://www.celphedia.eu/), especially the center AniRA-PBES of Lyon and the SCAR in addition to members of CIQLE imaging center (Faculté de Médecine Rockefeller, Lyon-Est), the contribution of SFR Biosciences (Universite Claude Bernard Lyon 1, CNRS UAR3444, Inserm US8, ENS de Lyon) Core Facility PLATIM, especially Elodie Chatre, for assistance with SIM technique. Human biological samples and associated data were obtained from Tissu-Tumorothèque Est Biobank (CRB-HCL Hospices Civils de Lyon BB-0033-00046) authorized by the French Ministry of Research. (Collection Number CRB HCL: DC2019-3464).

Author contribution

Nathalie Couturier: conceptualization, formal analysis, investigation, methodology, writing original draft
Léa Castellano: conceptualization, formal analysis, investigation, methodology, writing original draft
Alireza Ghasemizadeh: formal analysis, investigation, methodology
Emilie Christin: methodology
Céline Malleval: formal analysis, methodology
Alexandre Janin: ressources, methodology
Gaëtan Juban: ressources, methodology
Alexis Osseni: formal analysis, methodology
Jean Luc Thomas: methodology
Stéphane Konig: ressources, methodology
Jessica Brunetti: ressources, methodology
Alexandra Kraut: formal analysis, methodology
Yohann Couté: formal analysis, methodology
Nathalie Streichenberger: ressources
Rémi Mounier: ressources, investigation, methodology
Vincent Gache: conceptualization, formal analysis, supervision, funding acquisition, validation, investigation, visualization, methodology, writing original draft, project administration

All authors reviewed, edited, and approved the manuscript.

Disclosure and competing interest's statement

The authors declare no competing interests

COMPETING FINANCIAL INTERESTS

The authors declare no competing financial interests.

Bibliography

1. Metzger, T. *et al.* MAP and Kinesin dependent nuclear positioning is required for skeletal muscle function. *Nature* **484**, 120–124 (2012).

2. Roman, W. *et al.* Myofibril contraction and cross-linking drive nuclear movement to the periphery of skeletal muscle. *Nat. cell Biol.* **19**, 1189–1201 (2017).

3. Lele, T. P., Dickinson, R. B. & Gundersen, G. G. Mechanical principles of nuclear shaping and positioning. *J. Cell Biol.* **217**, 3330–3342 (2018).

4. Deshpande, O. & Telley, I. A. Nuclear positioning during development: Pushing, pulling and flowing. *Semin. Cell Dev. Biol.* **120**, 10–21 (2021).

5. Brodu, V., Baffet, A. D., Droguen, P.-M. L., Casanova, J. & Guichet, A. A Developmentally Regulated Two-Step Process Generates a Noncentrosomal Microtubule Network in Drosophila Tracheal Cells. *Dev. Cell* **18**, 790–801 (2010).

6. Efimov, A. *et al.* Asymmetric CLASP-Dependent Nucleation of Noncentrosomal Microtubules at the trans-Golgi Network. *Dev. Cell* **12**, 917–930 (2007).

7. Wilkes, O. R. & Moore, A. W. Distinct Microtubule Organizing Center Mechanisms Combine to Generate Neuron Polarity and Arbor Complexity. *Front. Cell. Neurosci.* **14**, 594199 (2020).

8. Cadot, B., Gache, V. & Gomes, E. R. Moving and positioning the nucleus in skeletal muscle – one step at a time. *Nucleus* **6**, 373–381 (2015).

9. Gache, V., Gomes, E. R. & Cadot, B. Microtubule motors involved in nuclear movement during skeletal muscle differentiation. *Mol. Biol. Cell* **28**, 865–874 (2017).

10. Rosen, J. N. *et al.* The Drosophila Ninein homologue Bsg25D cooperates with Ensconsin in myonuclear positioning. *J. Cell Biol.* **218**, 524–540 (2019).

11. Folker, E. S., Schulman, V. K. & Baylies, M. K. Muscle length and myonuclear position are independently regulated by distinct Dynein pathways. *Development* **139**, 3827–3837 (2012).

12. Espigat-Georger, A., Dyachuk, V., Chemin, C., Emorine, L. & Merdes, A. Nuclear alignment in myotubes requires centrosome proteins recruited by nesprin-1. *J. Cell Sci.* **129**, 4227–4237 (2016).

13. Ghasemizadeh, A. *et al.* MACF1 controls skeletal muscle function through the microtubule-dependent localization of extra-synaptic myonuclei and mitochondria biogenesis. *eLife* **10**, e70490 (2021).

14. Guiraud, A. *et al.* SH3KBP1 promotes skeletal myofiber formation and functionality through ER/SR architecture integrity. *EMBO Rep.* 1–26 (2025) doi:10.1038/s44319-025-00413-9.

15. Roman, W. *et al.* Muscle repair after physiological damage relies on nuclear migration for cellular reconstruction. *Science* **374**, 355–359 (2021).

16. Bruusgaard, J., Liestøl, K. & Gundersen, K. Distribution of myonuclei and microtubules in live muscle fibers of young, middle-aged, and old mice. *Journal of Applied Physiology* **100**, 2024–2030 (2006).

17. Romero, N. Centronuclear myopathies: a widening concept. *Neuromuscular disorders: NMD* **20**, 223–228 (2010).

18. Faber, R. M., Hall, J. K., Chamberlain, J. S. & Banks, G. B. Myofiber branching rather than myofiber hyperplasia contributes to muscle hypertrophy in mdx mice. *Skelet. Muscle* **4**, 10 (2014).

19. Falcone, S. *et al.* N-WASP is required for Amphiphysin-2/BIN1-dependent nuclear positioning and triad organization in skeletal muscle and is involved in the pathophysiology of centronuclear myopathy. *EMBO Mol. Med.* **6**, 1455–1475 (2014).

20. Prins, K. W. *et al.* Dystrophin is a microtubule-associated protein. *J. Cell Biol.* **186**, 363–369 (2009).

21. Oddoux, S. *et al.* Misplaced Golgi Elements Produce Randomly Oriented Microtubules and Aberrant Cortical Arrays of Microtubules in Dystrophic Skeletal Muscle Fibers. *Front. cell Dev. Biol.* **7**, 176 (2019).

22. Pimentel, M. R., Falcone, S., Cadot, B. & Gomes, E. R. In Vitro Differentiation of Mature Myofibers for Live Imaging. *Journal of visualized experiments: JoVE* e55141–e55141 (2017) doi:10.3791/55141.

23. Cadot, B. *et al.* Nuclear movement during myotube formation is microtubule and dynein dependent and is regulated by Cdc42, Par6 and Par3. *EMBO reports* **13**, 741–749 (2012).

24. Wang, Z. *et al.* Dissect Kif5b in nuclear positioning during myogenesis: The light chain binding domain and the autoinhibitory peptide are both indispensable. *Biochemical and biophysical research communications* **432**, 242–247 (2013).

25. Wilson, M. H. & Holzbaur, E. L. F. Nesprins anchor kinesin-1 motors to the nucleus to drive nuclear distribution in muscle cells. *Development* **142**, 218–228 (2014).

26. Gallini, S. *et al.* NuMA Phosphorylation by Aurora-A Orchestrates Spindle Orientation. *Curr. Biol.* **26**, 458–469 (2016).

27. Silk, A. D., Holland, A. J. & Cleveland, D. W. Requirements for NuMA in maintenance and establishment of mammalian spindle poles. *J. Cell Biol.* **184**, 677–690 (2009).

28. Radulescu, A. E. & Cleveland, D. W. NuMA after 30 years: the matrix revisited. *Trends in Cell Biology* **20**, 214–222 (2010).

29. Bugnard, E., Zaal, K. J. M. & Ralston, E. Reorganization of microtubule nucleation during muscle differentiation. *Cell Motil. Cytoskelet.* **60**, 1–13 (2005).

30. Haren, L. & Merdes, A. Direct binding of NuMA to tubulin is mediated by a novel sequence motif in the tail domain that bundles and stabilizes microtubules. *Journal of cell science* **115**, 1815–1824 (2002).

31. Kiyomitsu, T. & Cheeseman, I. M. Cortical dynein and asymmetric membrane elongation coordinately position the spindle in anaphase. *Cell* **154**, 391–402 (2013).

32. Gaglio, T., Saredi, A. & Compton, D. NuMA is required for the organization of microtubules into aster-like mitotic arrays. *J Cell Biology* **131**, 693–708 (1995).

33. Hueschen, C. L., Kenny, S. J., Xu, K. & Dumont, S. NuMA recruits dynein activity to microtubule minus-ends at mitosis. *eLife* **6**, e29328 (2017).

34. Castellano, L., Caillol, D., Streichenberger, N. & Gache, V. Interplay between microtubule interactome, myonuclei mechanotransduction, and positioning in myopathies. *Nucleus* **16**, 2524909 (2025).

35. Cassimeris, L. & Spittle, C. Regulation of microtubule-associated proteins. *Int Rev Cytol* **210**, 163–226 (2001).

36. Matsumura, S. *et al.* ABL1 regulates spindle orientation in adherent cells and mammalian skin. *Nat. Commun.* **3**, 626 (2012).

37. Kettenbach, A. N. *et al.* Quantitative Phosphoproteomics Identifies Substrates and Functional Modules of Aurora and Polo-Like Kinase Activities in Mitotic Cells. *Sci. Signal.* **4**, rs5 (2011).

38. Compton, D. A. & Luo, C. Mutation of the predicted p34cdc2 phosphorylation sites in numa impair the assembly of the mitotic spindle and block mitosis. *J. Cell Sci.* **108**, 621–633 (1995).

39. Schaffer, B. E. *et al.* Identification of AMPK Phosphorylation Sites Reveals a Network of Proteins Involved in Cell Invasion and Facilitates Large-Scale Substrate Prediction. *Cell metabolism* **22**, 907–921 (2015).

40. Theret, M. *et al.* AMPKα1-LDH pathway regulates muscle stem cell self-renewal by controlling metabolic homeostasis. *Embo J* **36**, 1946–1962 (2017).

41. Garry, G. A., Antony, M. & Garry, D. J. Cardiotoxin Induced Injury and Skeletal Muscle Regeneration. in vol. 1460 61–71 (Springer New York, 2016).

42. Bultot, L. *et al.* Benzimidazole derivative small-molecule 991 enhances AMPK activity and glucose uptake induced by AICAR or contraction in skeletal muscle. *Am. J. Physiol.-Endocrinol. Metab.* **311**, E706–E719 (2016).

43. Dong, X. *et al.* Metformin Increases Sarcolemma Integrity and Ameliorates Neuromuscular Deficits in a Murine Model of Duchenne Muscular Dystrophy. *Front. Physiol.* **12**, 642908 (2021).

44. Ljubicic, V. & Jasmin, B. J. AMP-activated protein kinase at the nexus of therapeutic skeletal muscle plasticity in Duchenne muscular dystrophy. *Trends Mol. Med.* **19**, 614–624 (2013).

45. Ljubicic, V. *et al.* Chronic AMPK activation evokes the slow, oxidative myogenic program and triggers beneficial adaptations in mdx mouse skeletal muscle. *Hum. Mol. Genet.* **20**, 3478–3493 (2011).

46. Desguerre, I. *et al.* A new model of experimental fibrosis in hindlimb skeletal muscle of adult mdx mouse mimicking muscular dystrophy. *Muscle Nerve* **45**, 803–814 (2012).

47. Zhou, G. *et al.* Role of AMP-activated protein kinase in mechanism of metformin action. *J. Clin. Investig.* **108**, 1167–1174 (2001).

48. Lemos, C. *et al.* The potent AMPK inhibitor BAY-3827 shows strong efficacy in androgen-dependent prostate cancer models. *Cell Oncol* **44**, 581–594 (2021).

49. Sanger, J. W., Wang, J., Fan, Y., White, J. & Sanger, J. M. Assembly and dynamics of myofibrils. *Journal of biomedicine \& biotechnology* **2010**, 858606–8 (2010).

50. Cho, S., Irianto, J. & Discher, D. E. Mechanosensing by the nucleus: From pathways to scaling relationships. *The Journal of cell biology* **216**, 305–315 (2017).

51. Santos, M. D. *et al.* Single-nucleus RNA-seq and FISH identify coordinated transcriptional activity in mammalian myofibers. *Nat. Commun.* **11**, 5102 (2020).

52. Iyer, S. R. *et al.* Altered nuclear dynamics in MDX myofibers. *J. Appl. Physiol.* **122**, 470–481 (2016).

53. Rajeevan, A., Keshri, R., Kapoor, S. & Kotak, S. NuMA interaction with chromatin is vital for proper chromosome decondensation at the mitotic exit. *Mol. Biol. Cell* **31**, 2437–2451 (2020).

54. Pascal, A., Gallaud, E., Giet, R. & Benaud, C. Annexin A2 and Ahnak control cortical NuMA-dynein localization and mitotic spindle orientation. *J. cell Sci.* **135**, (2021).

55. Serra-Marques, A. *et al.* The mitotic protein NuMA plays a spindle-independent role in nuclear formation and mechanics. *The Journal of cell biology* **219**, 348 (2020).

56. Merdes, A. & Cleveland, D. W. The role of NuMA in the interphase nucleus. *J Cell Sci* **111**, 71–79 (1998).

57. Capizzi, M. *et al.* Developmental defects in Huntington's disease show that axonal growth and microtubule reorganization require NUMA1. *Neuron* **110**, 36-50.e5 (2022).

58. Sun, Q.-Y. & Schatten, H. Role of NuMA in vertebrate cells: review of an intriguing multifunctional protein. *Frontiers in bioscience : a journal and virtual library* **11**, 1137–1146 (2006).

59. Harborth, J., Wang, J., Gueth-Hallonet, C., Weber, K. & Osborn, M. Self assembly of NuMA: multiarm oligomers as structural units of a nuclear lattice. *Embo J* **18**, 1689–1700 (1999).

60. Chandramouly, G., Abad, P. C., Knowles, D. W. & Lelièvre, S. A. The control of tissue architecture over nuclear organization is crucial for epithelial cell fate. *J Cell Sci* **120**, 1596–1606 (2007).

61. Simon, D. N. & Wilson, K. L. The nucleoskeleton as a genome-associated dynamic "network of networks". *Nature reviews. Molecular cell biology* **12**, 695–708 (2011).

62. Rodrigues, M., Echigoya, Y., Fukada, S.-I. & Yokota, T. Current Translational Research and Murine Models For Duchenne Muscular Dystrophy. *Journal of neuromuscular diseases* **3**, 29–48 (2016).

63. Randazzo, D. *et al.* Persistent upregulation of the β-tubulin tubb6, linked to muscle regeneration, is a source of microtubule disorganization in dystrophic muscle. *Hum. Mol. Genet.* **28**, 1117–1135 (2019).

64. Saclier, M. *et al.* Myofiber / pro-inflammatory macrophage interplay controls muscle damage in mdx mice. *J. Cell Sci.* **134**,.

65. Caratti, G. *et al.* Macrophagic AMPKα1 orchestrates regenerative inflammation induced by glucocorticoids. *EMBO Rep.* **24**, e55363 (2023).

66. Juban, G. *et al.* AMPK Activation Regulates LTBP4-Dependent TGF-β1 Secretion by Pro-inflammatory Macrophages and Controls Fibrosis in Duchenne Muscular Dystrophy. *Cell Rep.* **25**, 2163-2176.e6 (2018).

67. Chapman, V. M., Miller, D. R., Armstrong, D. & Caskey, C. T. Recovery of induced mutations for X chromosome-linked muscular dystrophy in mice. *Proc. Natl. Acad. Sci.* **86**, 1292–1296 (1989).

68. Laumonier, T., Koenig, S., Saüc, S. & Frieden, M. Isolation of Human Myoblasts, Assessment of Myogenic Differentiation, and Store-operated Calcium Entry Measurement. *J. Vis. Exp.* (2017) doi:10.3791/55918.

69. Brunetti, J., Koenig, S., Monnier, A. & Frieden, M. Nanopattern surface improves cultured human myotube maturation. *Skelet. Muscle* **11**, 12 (2021).

70. Gache, V., Waridel, P., Luche, S., Shevchenko, A. & Popov, A. V. Microtubule Protocols. *Methods Mol. Med.* **137**, 29–43 (2007).

71. Brinkley, B. R. Microtubule Organizing Centers. *Annu. Rev. Cell Dev. Biol.* **1**, 145–172 (1985).

72. Casabona, M. G., Vandenbrouck, Y., Attree, I. & Couté, Y. Proteomic characterization of Pseudomonas aeruginosa PAO1 inner membrane. *PROTEOMICS* **13**, 2419–2423 (2013).

73. Bouyssié, D. *et al.* Proline: an efficient and user-friendly software suite for large-scale proteomics. *Bioinformatics* **36**, 3148–3155 (2020).

74. Couté, Y., Bruley, C. & Burger, T. Beyond Target–Decoy Competition: Stable Validation of Peptide and Protein Identifications in Mass Spectrometry-Based Discovery Proteomics. *Anal. Chem.* **92**, 14898–14906 (2020).

75. Cadot, B., Gache, V. & Gomes, E. R. Fast, Multi-Dimensional and Simultaneous Kymograph-Like Particle Dynamics (SkyPad) Analysis. *PLoS ONE* **9**, e89073 (2014).

76. Sbalzarini, I. & Koumoutsakos, P. Feature point tracking and trajectory analysis for video imaging in cell biology. *J. Struct. Biol.* **151**, 182–195 (2005).

77. Liu, W. & Ralston, E. A new directionality tool for assessing microtubule pattern alterations. *Cytoskeleton* **71**, 230–240 (2014).

Figure 1

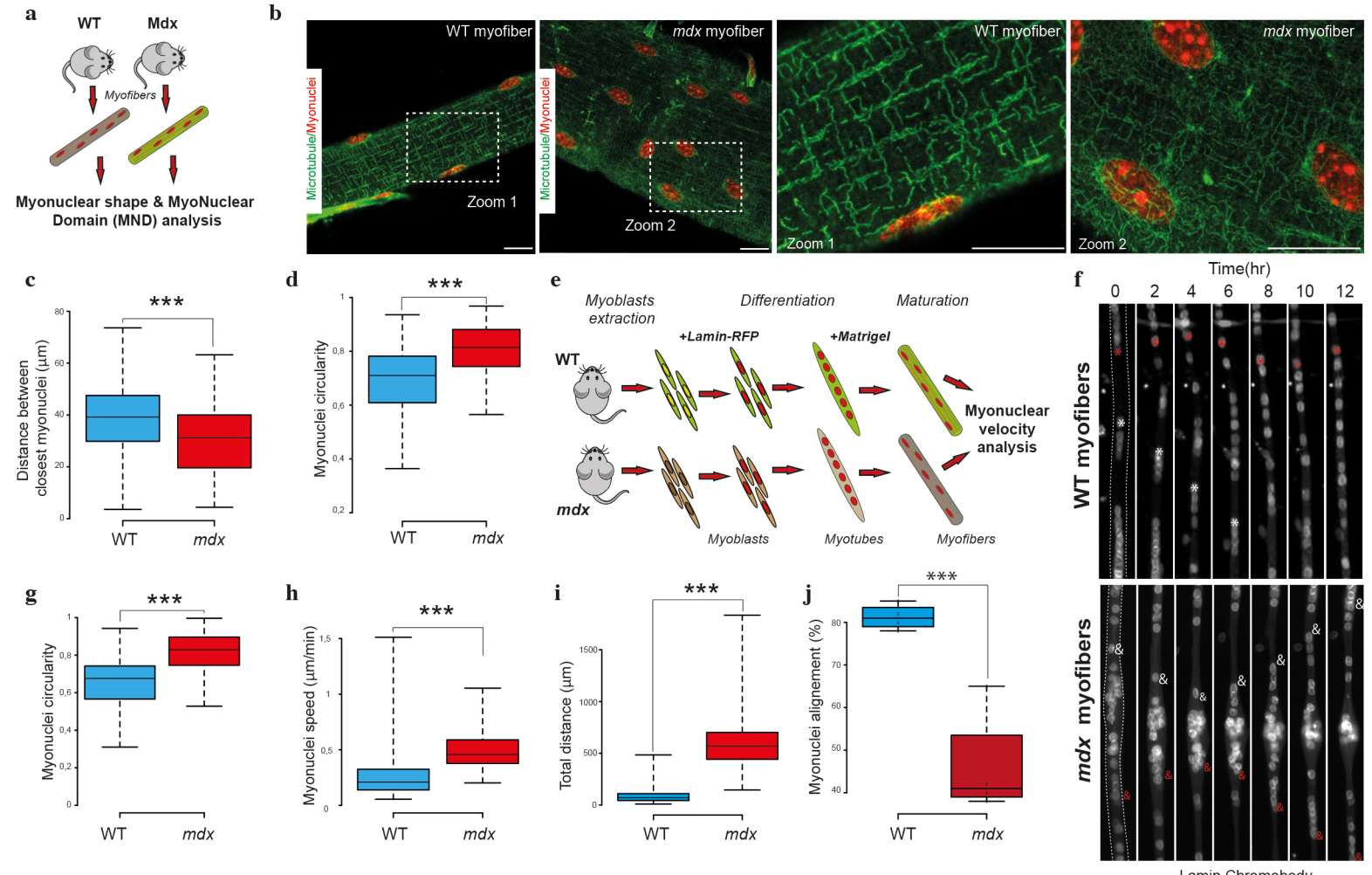

a
WT
Mdx
Myofibers
Myonuclear shape & MyoNuclear Domain (MND) analysis
b
WT myofiber
mdx myofiber
Microtubule/Myonuclei
Zoom 1
Zoom 2
c
Distance between closest myonuclei (µm)
***
WT
mdx
d
Myonuclei circularity
e
Myoblasts extraction
Differentiation
Maturation
+Lamin-RFP
+Matrigel
WT
mdx
Myonuclear velocity analysis
Myoblasts
Myotubes
Myofibers
f
Time(hr)
0 2 4 6 8 10 12
WT myofibers
mdx myofibers
Lamin Chromobody
g
Myonuclei circularity
h
Myonuclei speed (µm/min)
i
Total distance (µm)
j
Myonuclei alignement (%)

Figure 2

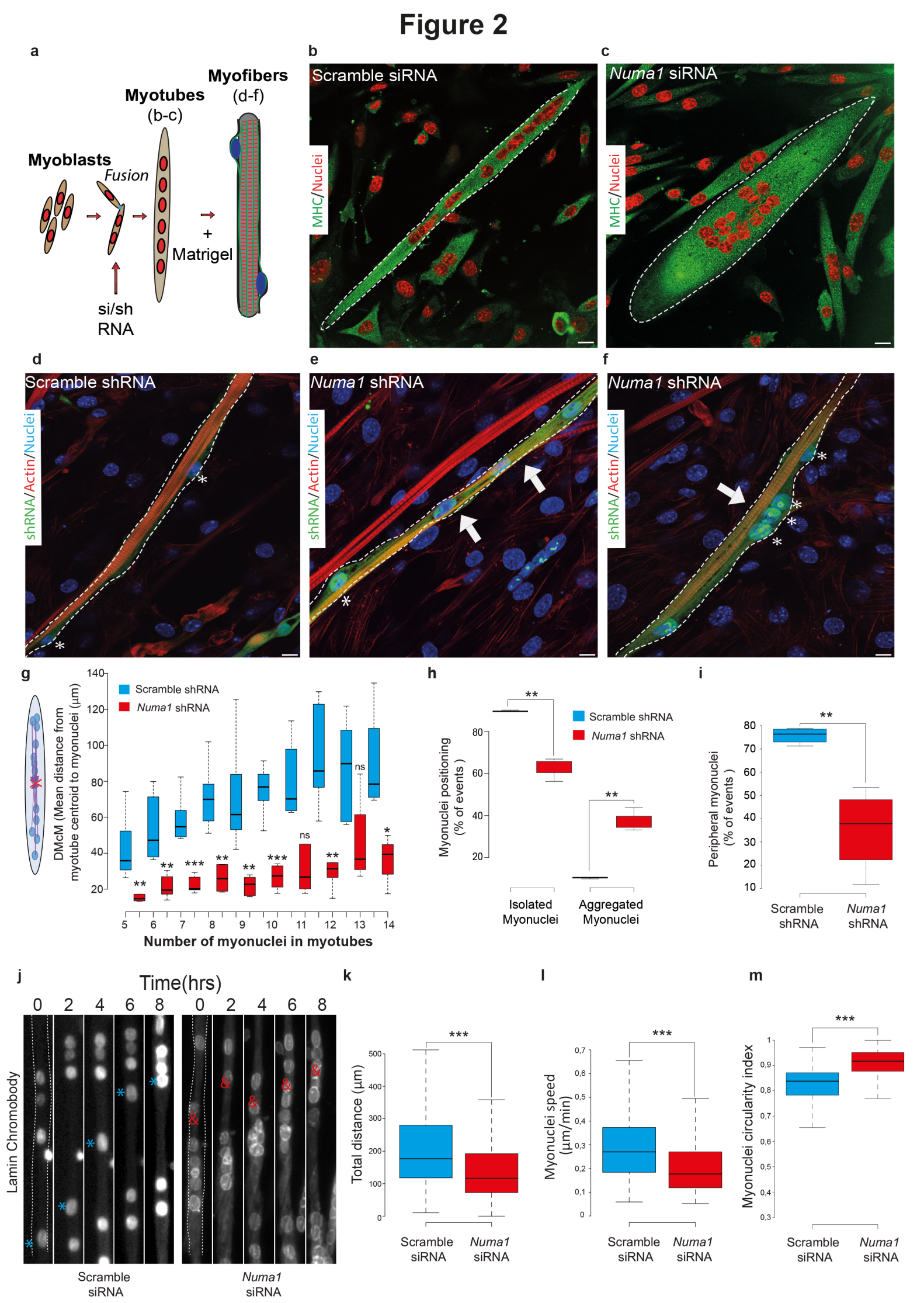

a
Myofibers
(d-f)
Myotubes
(b-c)
Myoblasts
Fusion
+
Matrigel
si/sh
RNA
b
Scramble siRNA
MHC/Nuclei
c
Numa1 siRNA
MHC/Nuclei
d
Scramble shRNA
shRNA/Actin/Nuclei
e
Numa1 shRNA
shRNA/Actin/Nuclei
f
Numa1 shRNA
shRNA/Actin/Nuclei
g
Scramble shRNA
Numa1 shRNA
DMcM (Mean distance from myotube centroid to myonuclei (µm)
Number of myonuclei in myotubes
h
Scramble shRNA
Numa1 shRNA
Myonuclei positioning (% of events)
Isolated Myonuclei
Aggregated Myonuclei
i
Peripheral myonuclei (% of events)
Scramble shRNA
Numa1 shRNA
j
Time(hrs)
0 2 4 6 8 0 2 4 6 8
Lamin Chromobody
Scramble siRNA
Numa1 siRNA
k
Total distance (µm)
Scramble siRNA
Numa1 siRNA
l
Myonuclei speed (µm/min)
Scramble siRNA
Numa1 siRNA
m
Myonuclei circularity index
Scramble siRNA
Numa1 siRNA

Figure 3

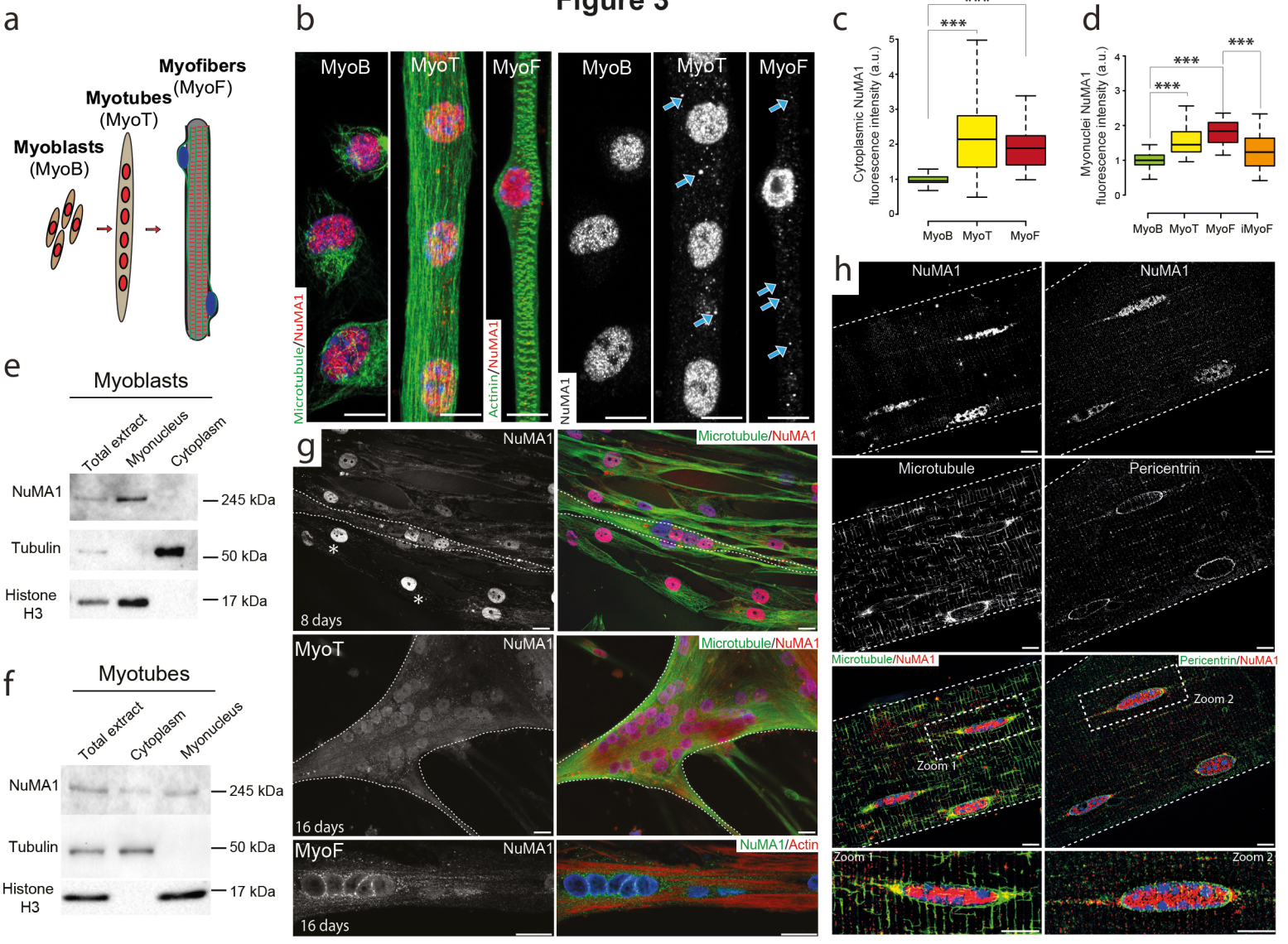

a
Myofibers (MyoF)
Myotubes (MyoT)
Myoblasts (MyoB)
b
MyoB
MyoT
MyoF
Microtubule/NuMA1
Actinin/NuMA1
NuMA1
c
Cytoplasmic NuMA1 fluorescence intensity (a.u.)
***
MyoB MyoT MyoF
d
Myonuclei NuMA1 fluorescence intensity (a.u.)
***
MyoB MyoT MyoF iMyoF
e
Myoblasts
Total extract
Myonucleus
Cytoplasm
NuMA1
Tubulin
Histone H3
245 kDa
50 kDa
17 kDa
f
Myotubes
Total extract
Cytoplasm
Myonucleus
NuMA1
Tubulin
Histone H3
245 kDa
50 kDa
17 kDa
g
NuMA1
Microtubule/NuMA1
8 days
MyoT
16 days
MyoF
NuMA1/Actin
h
NuMA1
Microtubule
Pericentrin
Microtubule/NuMA1
Pericentrin/NuMA1
Zoom 1
Zoom 2

Figure 4

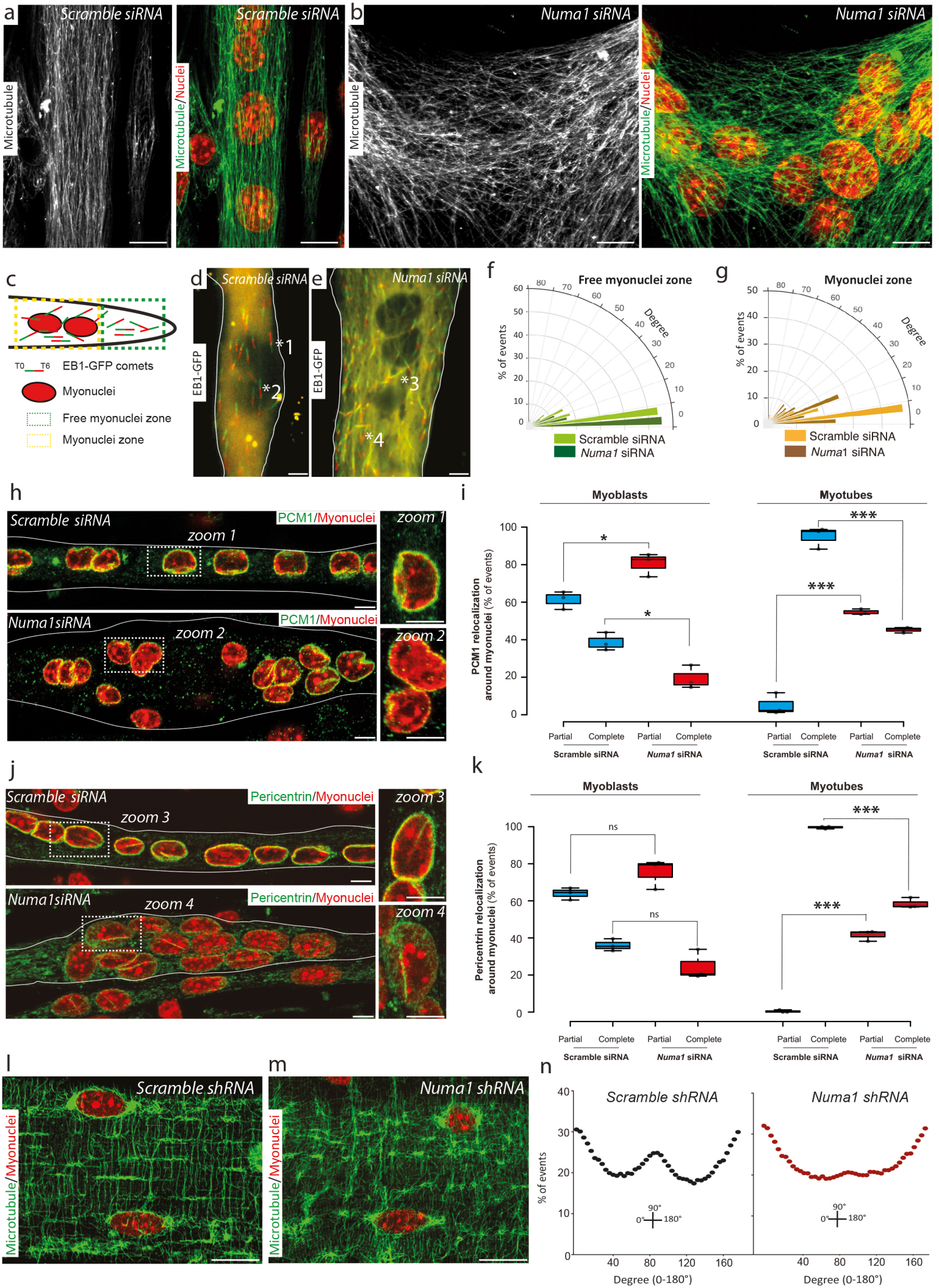

a
Scramble siRNA
Microtubule
Scramble siRNA
Microtubule/Nuclei
b
Numa1 siRNA
Microtubule
Numa1 siRNA
Microtubule/Nuclei
c
T0 T6 EB1-GFP comets
Myonuclei
Free myonuclei zone
Myonuclei zone
d
Scramble siRNA
EB1-GFP
*1
*2
e
Numa1 siRNA
EB1-GFP
*3
*4
f
Free myonuclei zone
% of events
Degree
Scramble siRNA
Numa1 siRNA
g
Myonuclei zone
% of events
Degree
Scramble siRNA
Numa1 siRNA
h
Scramble siRNA
PCM1/Myonuclei
zoom 1
zoom 1
Numa1siRNA
PCM1/Myonuclei
zoom 2
zoom 2
i
Myoblasts
Myotubes
PCM1 relocalization around myonuclei (% of events)
Partial Complete Partial Complete
Scramble siRNA
Numa1 siRNA
j
Scramble siRNA
Pericentrin/Myonuclei
zoom 3
zoom 3
Numa1siRNA
Pericentrin/Myonuclei
zoom 4
zoom 4
k
Myoblasts
Myotubes
Pericentrin relocalization around myonuclei (% of events)
ns
Partial Complete Partial Complete
Scramble siRNA
Numa1 siRNA
l
Scramble shRNA
Microtubule/Myonuclei
m
Numa1 shRNA
Microtubule/Myonuclei
n
Scramble shRNA
Numa1 shRNA
% of events
90°
0°
180°
Degree (0-180°)

Figure 5

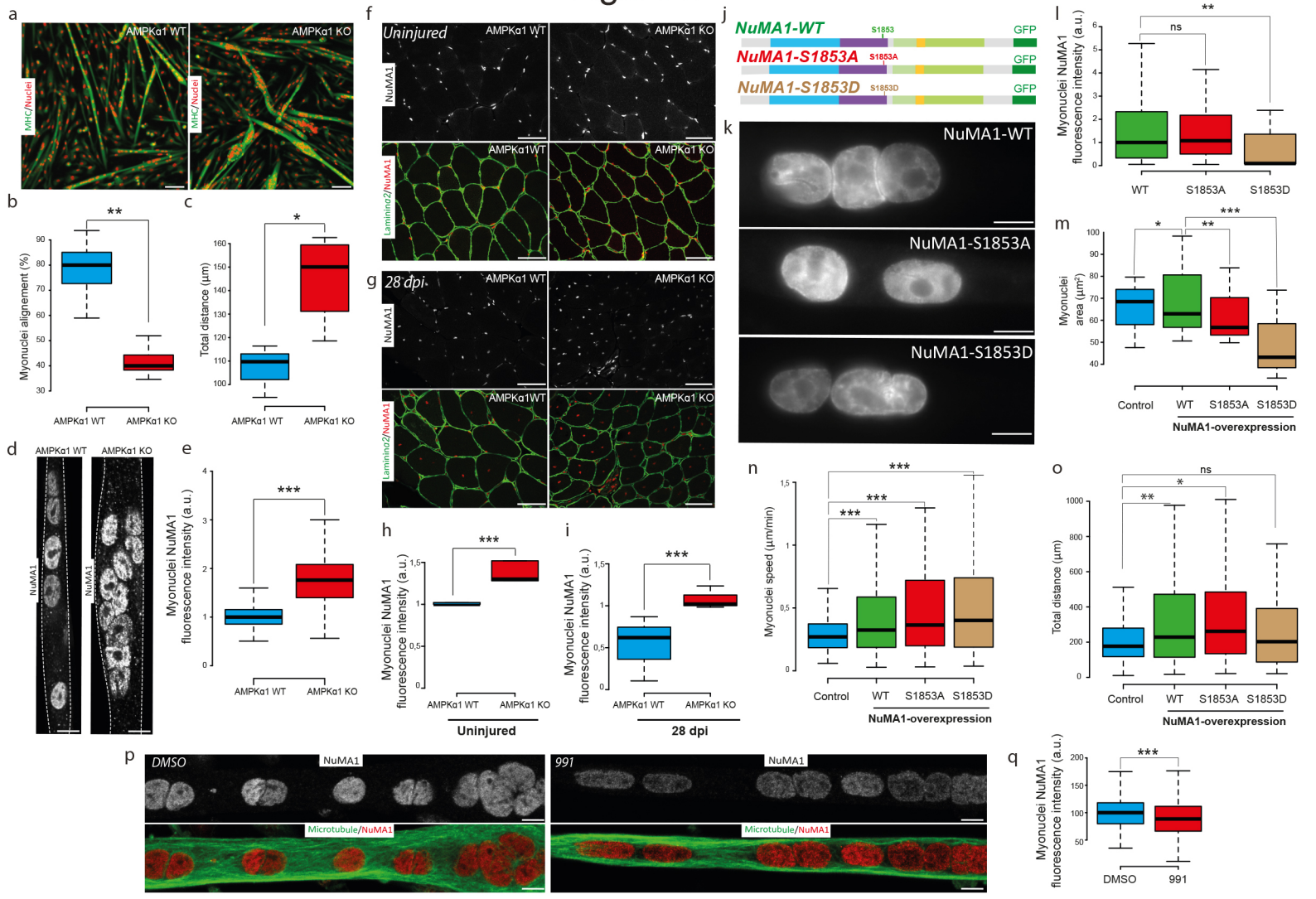
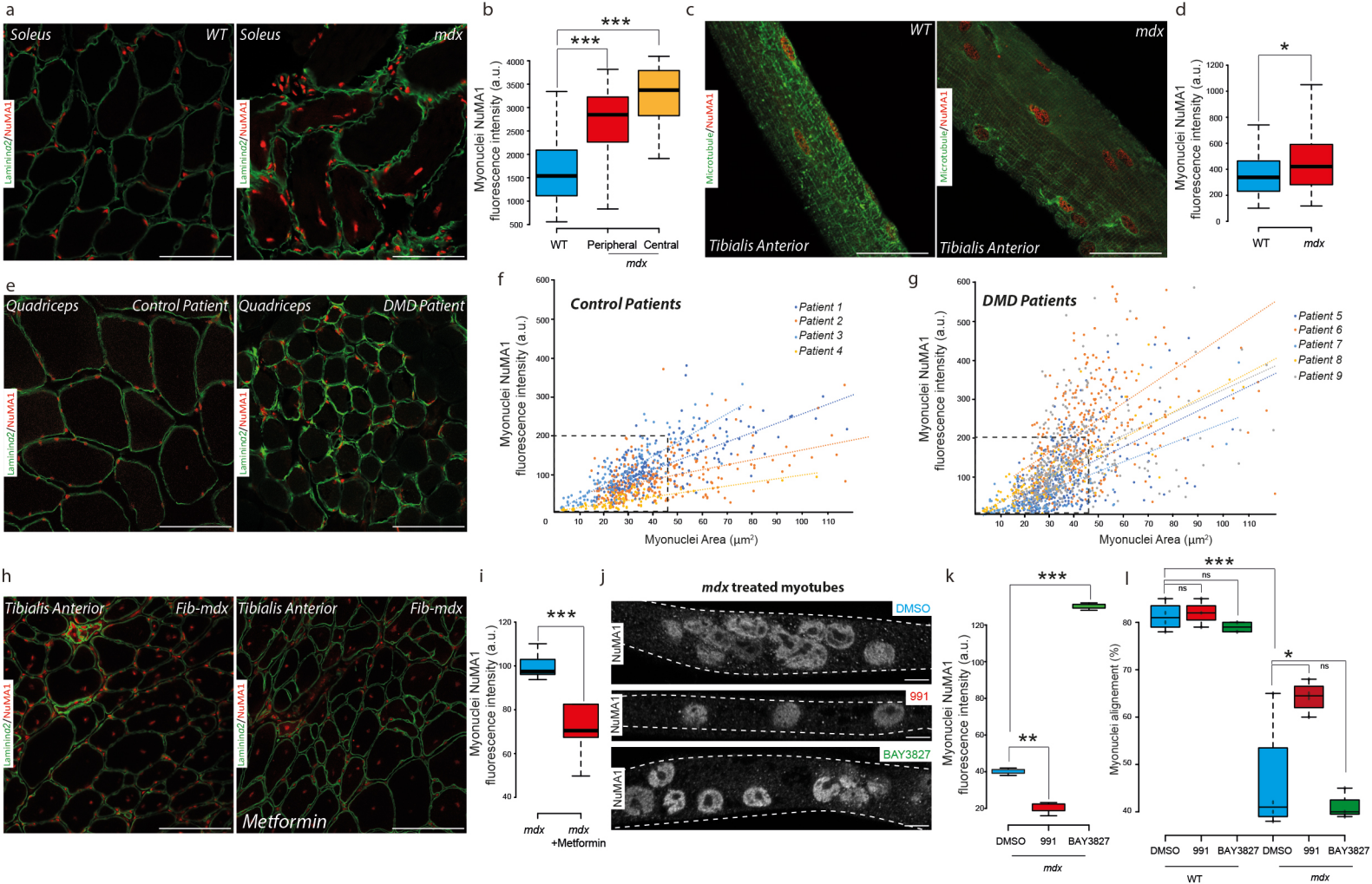
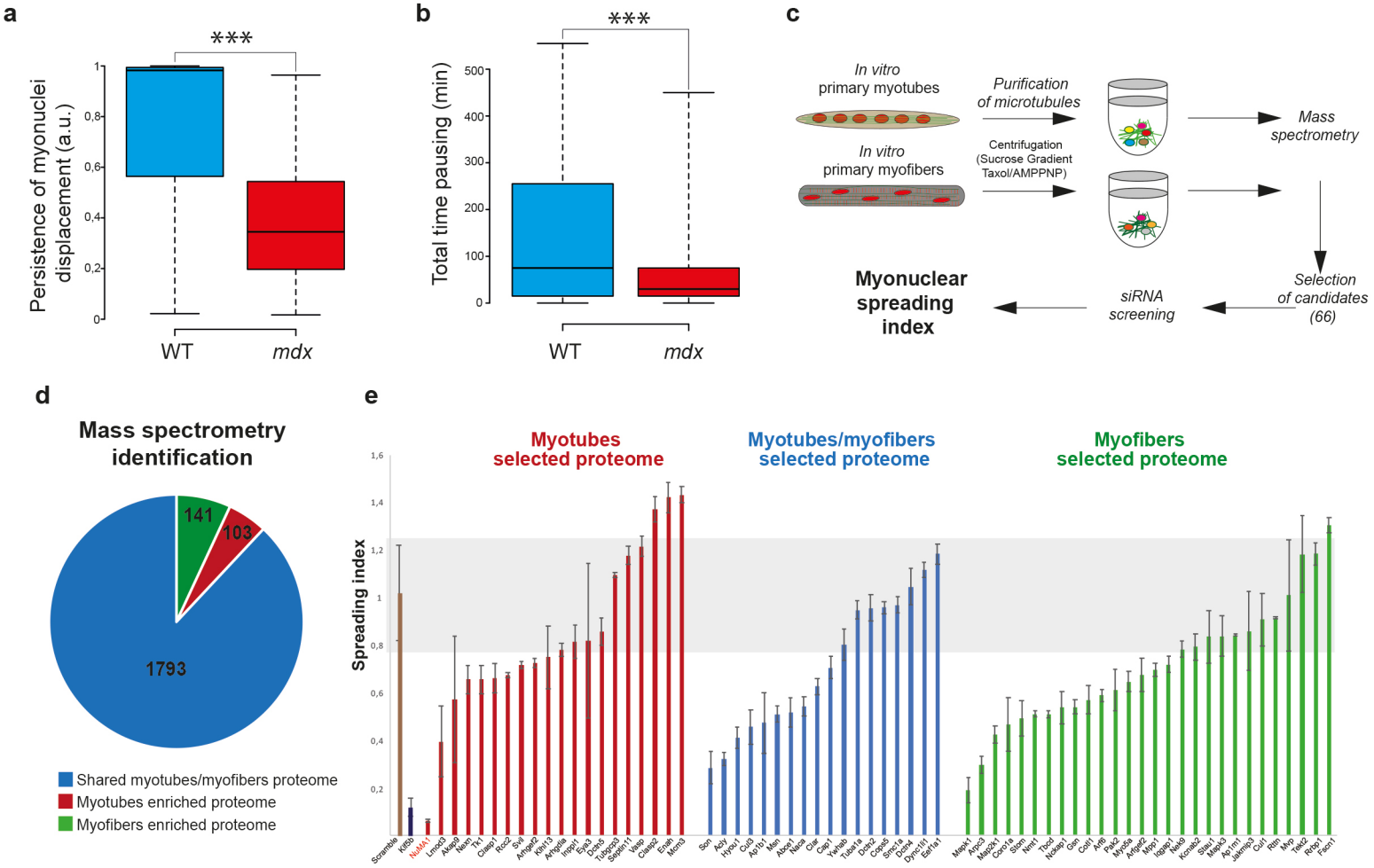

a
AMPKα1 WT
AMPKα1 KO
MHC/Nuclei
b
Myonuclei alignement (%)
AMPKα1 WT
AMPKα1 KO
c
Total distance (µm)
d
NuMA1
e
Myonuclei NuMA1 fluorescence intensity (a.u.)
f
Uninjured
NuMA1
Laminin2/NuMA1
g
28 dpi
h
Uninjured
i
28 dpi
j
NuMA1-WT
NuMA1-S1853A
NuMA1-S1853D
S1853
GFP
k
l
Myonuclei NuMA1 fluorescence intensity (a.u.)
ns
WT
S1853A
S1853D
m
Myonuclei area (µm²)
Control
NuMA1-overexpression
n
Myonuclei speed (µm/min)
o
Total distance (µm)
p
DMSO
991
Microtubule/NuMA1
q
Myonuclei NuMA1 fluorescence intensity (a.u.)

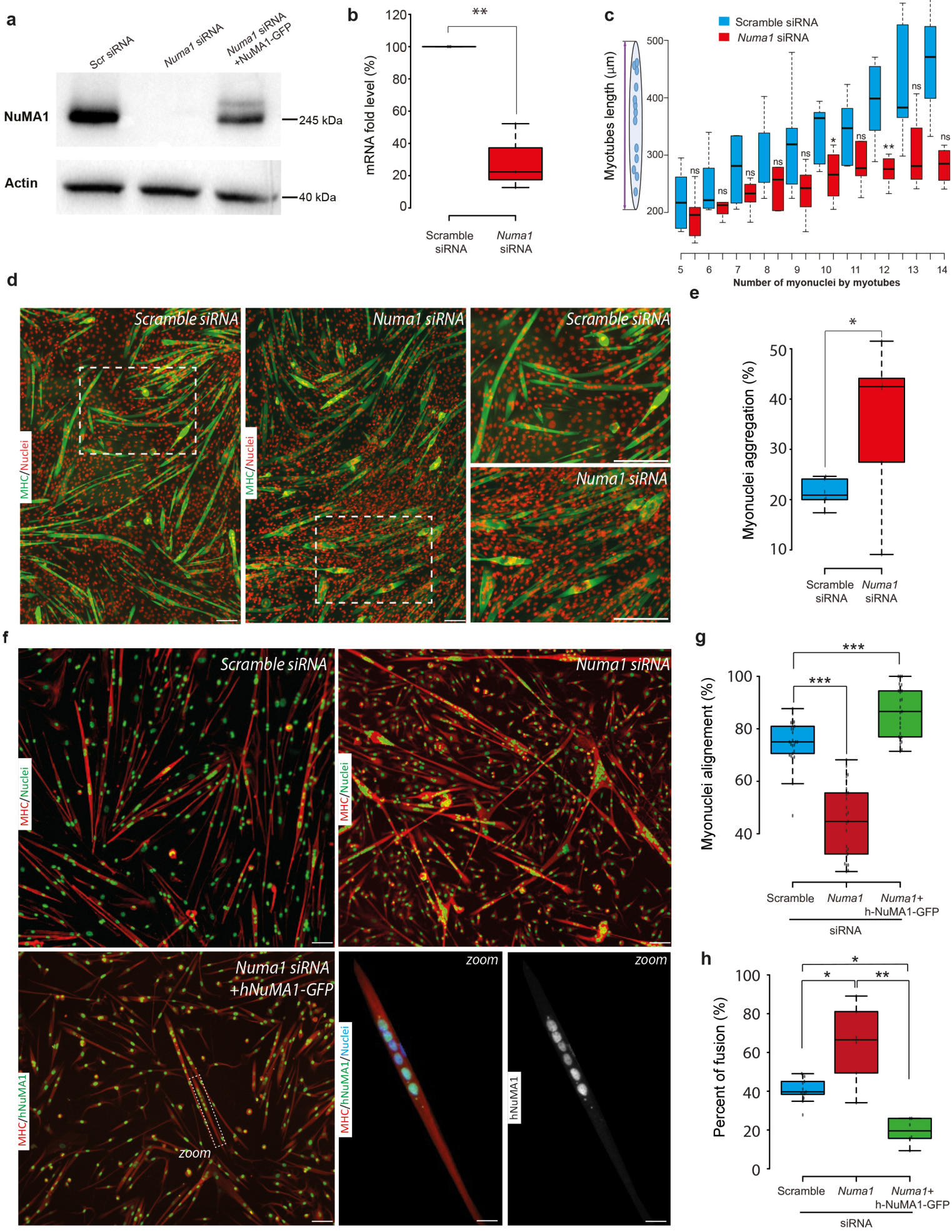
Figure 6


a
Soleus
WT
Soleus
mdx
Laminin α2/NuMA1
b
***
***
Myonuclei NuMA1 fluorescence intensity (a.u.)
WT
Peripheral
Central
mdx
c
WT
mdx
Microtubule/NuMA1
Tibialis Anterior
Tibialis Anterior
d
*
Myonuclei NuMA1 fluorescence intensity (a.u.)
WT
mdx
e
Quadriceps
Control Patient
Quadriceps
DMD Patient
f
Control Patients
Patient 1
Patient 2
Patient 3
Patient 4
Myonuclei NuMA1 fluorescence intensity (a.u.)
Myonuclei Area (μm²)
g
DMD Patients
Patient 5
Patient 6
Patient 7
Patient 8
Patient 9
Myonuclei NuMA1 fluorescence intensity (a.u.)
Myonuclei Area (μm²)
h
Tibialis Anterior
Fib-mdx
Tibialis Anterior
Fib-mdx
Metformin
i
***
Myonuclei NuMA1 fluorescence intensity (a.u.)
mdx
mdx +Metformin
j
mdx treated myotubes
DMSO
991
BAY3827
NuMA1
k
***
**
Myonuclei NuMA1 fluorescence intensity (a.u.)
DMSO
991
BAY3827
mdx
l
***
ns
ns
*
ns
Myonuclei alignement (%)
DMSO
991
BAY3827
DMSO
991
BAY3827
WT
mdx

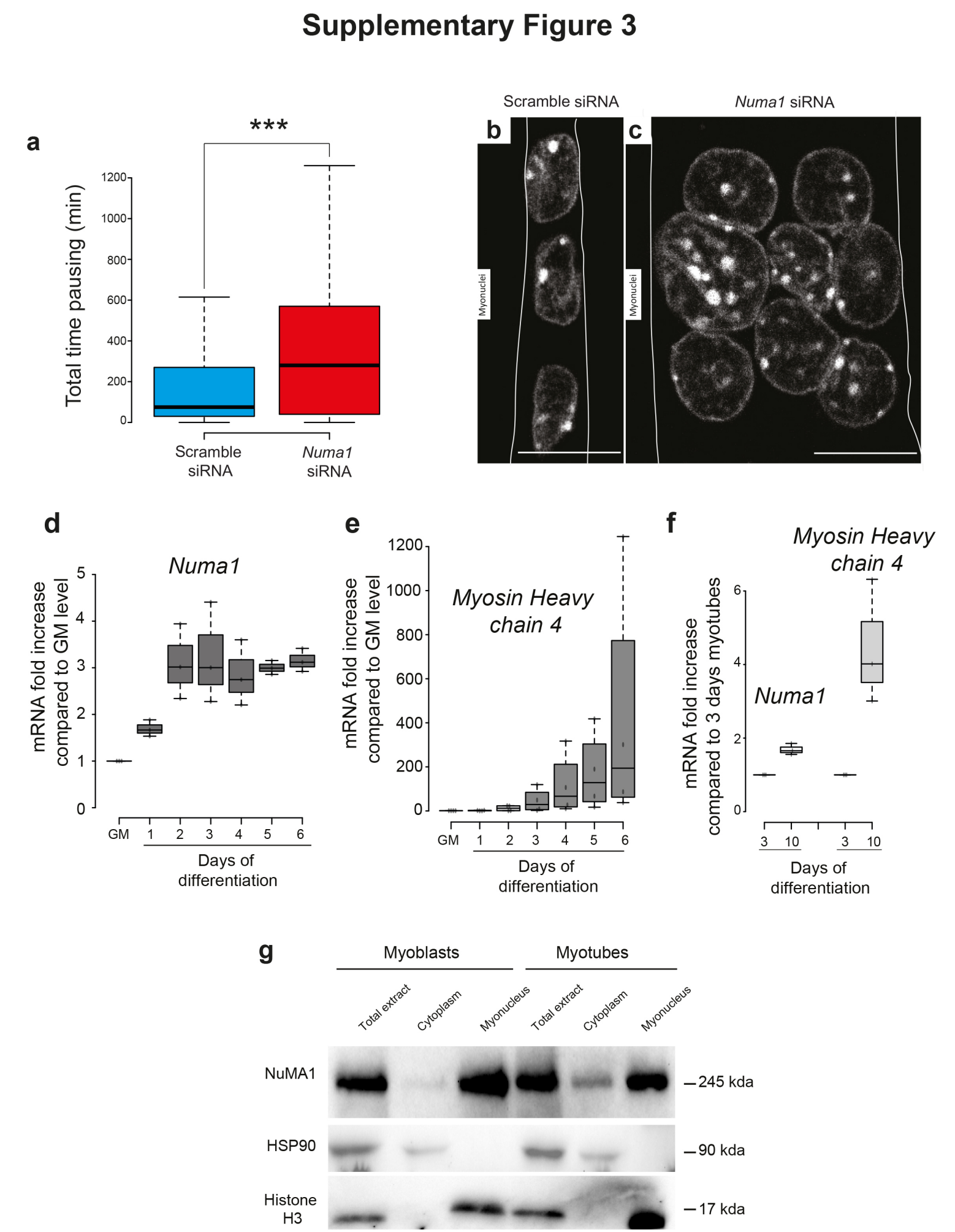
Supplementary Figure 1



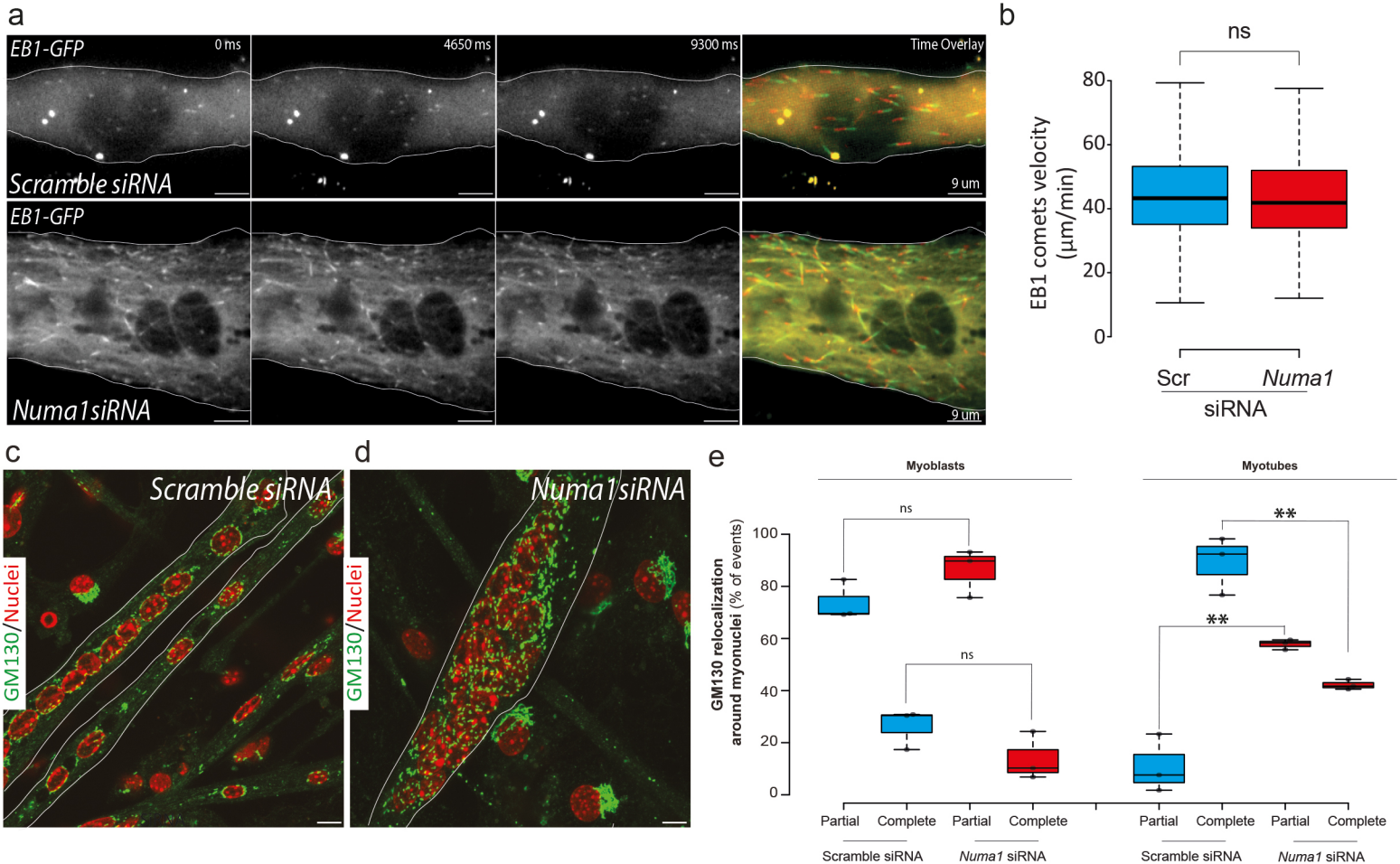
Supplementary Figure 2



Supplementary Figure 3



Supplementary Figure 4



Supplementary Figure 5

